Kynurenine monooxygenase regulates inflammation during critical illness and recovery in experimental acute pancreatitis

Cell Reports

Article

Kynurenine monooxygenase regulates inflammation during critical illness and recovery in experimental acute pancreatitis

Graphical abstract

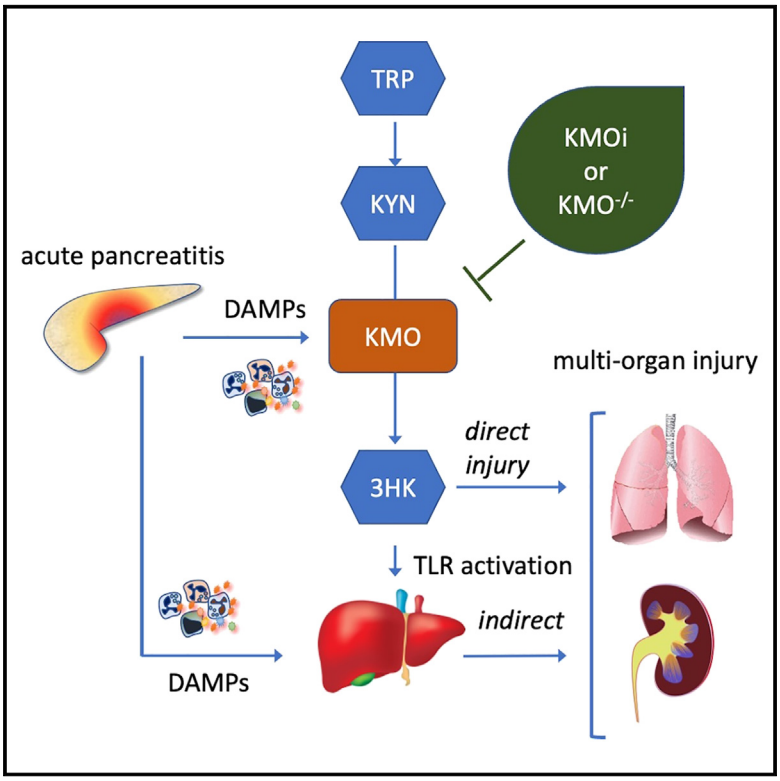

Highlights

- KMO activity primes innate immune and inflammatory gene transcription through 3HK production
- 3HK synergizes with interleukin-1β to cause cell apoptosis
- Therapeutic KMO blockade rescues fatal inflammation in experimental acute pancreatitis

Authors

Alastair J. Hayes, Xiaozhong Zheng, James O'Kelly, ..., John P. Iredale, Sarah E.M. Howie, Damian J. Mole

Correspondence

damian.mole@ed.ac.uk

In brief

Hayes et al. characterize a metabolic link between 3-hydroxykynurenine generated by KMO activity and priming of innate immune gene transcription during systemic inflammation. Therapeutic blockade using the highly specific KMO inhibitor GSK898 rescues the phenotype and protects against excess morbidity and death from multiple organ failure in experimental acute pancreatitis.

Hayes et al., 2023, Cell Reports *42*, 112763
August 29, 2023
https://doi.org/10.1016/j.celrep.2023.112763

CellPress

Cell Reports

CellPress
OPEN ACCESS

Article

Kynurenine monooxygenase regulates inflammation during critical illness and recovery in experimental acute pancreatitis

Alastair J. Hayes,[1,2,10] Xiaozhong Zheng,[1] James O'Kelly,[1,2] Lucile P.A. Neyton,[1,3] Natalia A. Bochkina,[4] Iain Uings,[5] John Liddle,[5] J. Kenneth Baillie,[3] George Just,[6] Margaret Binnie,[6] Natalie Z.M. Homer,[6] Toby B.J. Murray,[2] James Baily,[7] Kris McGuire,[1] Christos Skouras,[2] O. James Garden,[2] Scott P. Webster,[8] John P. Iredale,[9] Sarah E.M. Howie,[1] and Damian J. Mole[1,2,10,11,*]

[1]University of Edinburgh Centre for Inflammation Research, Institute for Regeneration and Repair, University of Edinburgh, Edinburgh, UK
[2]Clinical Surgery, University of Edinburgh, Edinburgh, UK
[3]The Roslin Institute, University of Edinburgh, Edinburgh, UK
[4]School of Mathematics and Maxwell Institute, University of Edinburgh, Edinburgh, UK
[5]GlaxoSmithKline, Gunnels Wood Road, Stevenage, Hertfordshire, UK
[6]Mass Spectrometry Core, Edinburgh Clinical Research Facility, University of Edinburgh, Edinburgh, UK
[7]Charles River Laboratories, East Lothian, UK
[8]Centre for Cardiovascular Science, University of Edinburgh, Edinburgh, UK
[9]University of Bristol, Bristol, UK
[10]Senior author
[11]Lead contact
*Correspondence: damian.mole@ed.ac.uk
https://doi.org/10.1016/j.celrep.2023.112763

SUMMARY

Kynurenine monooxygenase (KMO) blockade protects against multiple organ failure caused by acute pancreatitis (AP), but the link between KMO and systemic inflammation has eluded discovery until now. Here, we show that the KMO product 3-hydroxykynurenine primes innate immune signaling to exacerbate systemic inflammation during experimental AP. We find a tissue-specific role for KMO, where mice lacking *Kmo* solely in hepatocytes have elevated plasma 3-hydroxykynurenine levels that prime inflammatory gene transcription. 3-Hydroxykynurenine synergizes with interleukin-1β to cause cellular apoptosis. Critically, mice with elevated 3-hydroxykynurenine succumb fatally earlier and more readily to experimental AP. Therapeutically, blockade with the highly selective KMO inhibitor GSK898 rescues the phenotype, reducing 3-hydroxykynurenine and protecting against critical illness and death. Together, our findings establish KMO and 3-hydroxykynurenine as regulators of inflammation and the innate immune response to sterile inflammation. During critical illness, excess morbidity and death from multiple organ failure can be rescued by systemic KMO blockade.

INTRODUCTION

Acute pancreatitis (AP) is inflammation of the pancreas gland that initiates a rapid and clinically unpredictable systemic inflammatory response involving cytokines, damage-associated molecular pattern molecules (DAMPs), altered metabolic flux, and innate immune system activation that together can result in life-threatening systemic complications.[1,2] AP is triggered by gallstones or excess alcohol consumption and other rarer causes, including trauma. The worldwide incidence of AP is 34 per 100,000 person years[3] and is the most frequent gastrointestinal diagnosis for hospital admission in the USA.[4] The initial pathological event in AP is dysregulated intracellular calcium signaling in the pancreatic acinar cell, causing mitochondrial dysfunction and premature activation of digestive enzymes to result in cellular injury and release of DAMPs.[1,5] The inflammatory cascade that ensues is sufficiently severe in 1 in 5 individuals with AP to overwhelm homeostatic mechanisms resulting in multiple organ dysfunction syndrome (AP-MODS).[6] The severity of AP-MODS ranges from transient organ dysfunction to sustained organ failure, and the overall case fatality rate of AP-MODS is 22%.[7] More than half of deaths from AP occur within 1 week of disease onset as a result of overwhelming sterile systemic inflammation and failure of multiple organ systems.[8]

Increased flux through the kynurenine pathway of tryptophan metabolism (Figure 1A) is a critical component of the inflammatory cascade that contributes to AP-MODS.[9–11] In health, over 90% of free tryptophan is metabolized in the liver via the kynurenine pathway.[12,13] The flavoenzyme kynurenine 3-monooxygenase (KMO; E.C. 1.14.13.9) is a critical step in the kynurenine pathway. During inflammation, expression of the *Kmo* gene is upregulated,[14–16] and increased activity of the enzymes upstream of

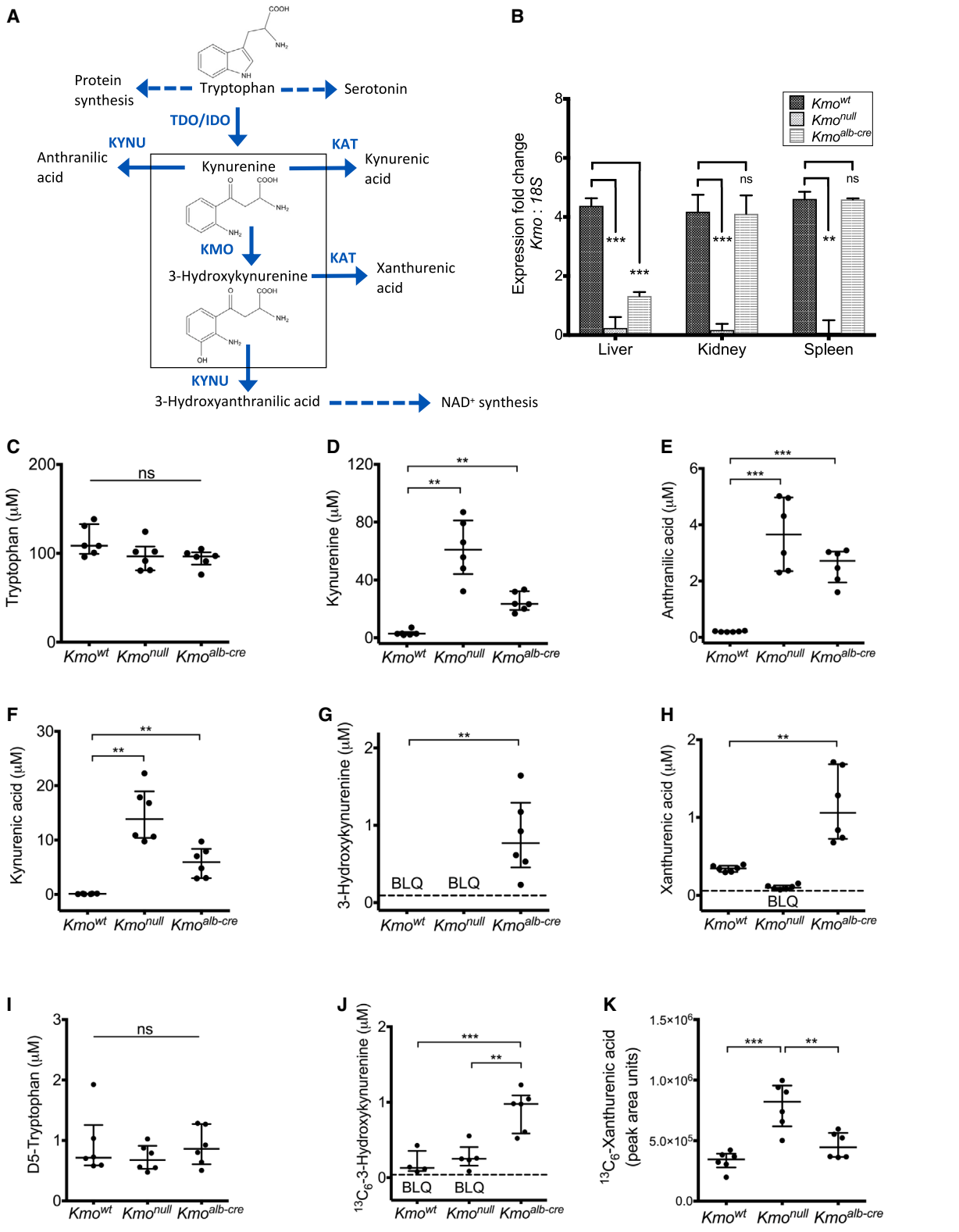

Figure 1. Biochemical characterization of a hepatocyte-restricted *Kmo* knockdown mouse line (*Kmo*$^{alb\text{-}cre}$)

(A) Kynurenine pathway schematic. Abbreviations: IDO, indolamine-2,3-dioxygenase; KAT, kynurenine aminotransferases; KMO, kynurenine 3-monooxygenase; KYNU, kynureninase; NAD$^+$, nicotinamide adenine dinucleotide (oxidized); TDO, tryptophan-2,3-dioxygenase.

(legend continued on next page)

KMO, namely indoleamine 2,3-dioxygenase 1 (IDO1; E.C. 1.13.11.52) and tryptophan 2,3-dioxygenase (TDO; E.C. 1.13.11.11), increases the availability of the KMO substrate, kynurenine, which together results in increased 3-hydroxykynurenine production.[14–16] 3-Hydroxykynurenine causes cellular injury by oxidative stress and pathological cross-linking of proteins and induction of apoptotic cell death.[17,18] Importantly, elevated 3-hydroxykynurenine concentrations correlate with disease severity in human AP.[9] Systemic KMO inhibition results in increased kynurenine levels and diversion of kynurenine metabolism to kynurenic acid,[19,20] and mice genetically engineered to lack *Kmo* in all tissues exhibit a similar plasma kynurenine metabolite profile to that seen when KMO activity is inhibited pharmacologically. Therapeutic KMO blockade abolishes 3-hydroxykynurenine production and protects against experimental AP-MODS in rats and mice.[10] However, the precise mechanisms by which KMO and 3-hydroxykynurenine regulate inflammation have remained elusive until now.

Our aim here was to elucidate the molecular mechanisms that underpin the protective effect of KMO inhibition in critical illness caused by AP and to define whether circulating 3-hydroxykynurenine produced by the liver during systemic inflammation was a dominant force in causing tissue damage to other organs, for example, lungs and kidneys, compared with 3-hydroxykynurenine produced in the local environment of those remotely injured tissues. When taken together, our findings establish that the KMO product 3-hydroxykynurenine generated in the periphery is a regulator of intracellular inflammatory signaling pathways and that, during critical illness, excess death from multiple organ failure can be rescued by systemic KMO blockade.

RESULTS

Restricting *Kmo* gene knockdown to hepatocytes constrains liver KMO activity but causes an elevation in circulating plasma 3-hydroxykynurenine levels

The organs most commonly damaged during AP-MODS are the lungs and kidneys, yet hepatocytes of the liver are the main site of kynurenine metabolism. We therefore questioned whether pathological 3-hydroxykynurenine in AP was produced locally in lungs and kidney tissue or arrived in plasma via systemic circulation. Using laboratory mice, our strategy was to knock down *Kmo* gene expression in hepatocytes, leaving *Kmo* gene expression intact in the rest of the body. Because the majority of KMO activity resides in the liver, we predicted an altered plasma biochemical phenotype similar to mice with *Kmo* deletion in all tissues. To test this, we generated a genetically altered mouse strain that lacks KMO activity in hepatocytes only by crossing $Kmo^{tm1c(KOMPWtsi/flox(ex5)}$ mice (which have *loxP* sites flanking exon 5 of the *Kmo* gene) with a mouse strain that expresses Cre recombinase under the control of the promoter for the *Alb* gene (which encodes the protein serum albumin), B6.Cg-Tg (*Alb*-Cre) 21Mgn/J, and expresses Cre recombinase exclusively in hepatocytes. Offspring were further backcrossed for at least 6 generations to generate homozygous $Kmo^{FRT\text{-}deleted/alb\text{-}cre}$ mice (hereafter referred to as $Kmo^{alb\text{-}cre}$ mice). Liver-specific suppression of *Kmo* mRNA in $Kmo^{alb\text{-}cre}$ mice was confirmed by RT-PCR, showing equivalent expression in kidney and spleen to wild-type controls (Kmo^{WT} mice) but significantly reduced *Kmo* expression in whole liver tissue homogenate detected at low levels, but not to undetectable levels, as was observed in mice with *Kmo* knockout in all tissues (termed Kmo^{null} mice) (Figure 1B). Steady-state levels of plasma kynurenine pathway metabolites were measured by liquid chromatography-tandem mass spectrometry (LC/MS-MS) in $Kmo^{alb\text{-}cre}$ mice and compared with WT mice (Kmo^{WT}) and with the global *Kmo* knockout mouse line control (Kmo^{null}). Plasma tryptophan concentrations (Figure 1C) were not different between all three mouse lines ($p = 0.075$, one-way analysis of variance [ANOVA]), whereas Kmo^{null} mice had a 21-fold increase in plasma kynurenine levels compared with Kmo^{WT} mice (median 60.9 vs. 2.8 μM, $p = 0.002$, Mann-Whitney test), and $Kmo^{alb\text{-}cre}$ mice had an 8-fold increase in plasma kynurenine compared with Kmo^{WT} mice (median 23.4 vs. 2.8 μM, $p = 0.002$, Mann-Whitney test) (Figure 1D). A corresponding increase in plasma anthranilic acid was present in Kmo^{null} mice (18-fold increase, median 3.6 vs. 0.2 μM, $p = 0.001$, t test) and $Kmo^{alb\text{-}cre}$ mice (14-fold increase, median 2.7 vs. 0.2 μM, $p < 0.001$, t test) compared with Kmo^{WT} mice (Figure 1E). As we previously observed, excess plasma kynurenine is readily converted to kynurenic acid if KMO activity is blocked, and in these experiments, Kmo^{null} mice had a 115-fold excess (median 13.9 vs. 0.1 μM, $p = 0.002$, Mann-Whitney test) compared with Kmo^{WT} mice.[10] Similarly, excess kynurenine in $Kmo^{alb\text{-}cre}$ mice was metabolized to kynurenic acid, and these mice had a 50-fold increase in kynurenic acid levels (median 5.9 vs. 0.1 μM, $p = 0.002$, Mann-Whitney test)

(B) mRNA tissue expression in liver, kidney, and spleen of Kmo^{WT}, Kmo^{null}, and $Kmo^{alb\text{-}cre}$ mice (n = 5 per group). Fold increase compared with 18S mRNA control expression levels. Bars are median with interquartile range (IQR). Group statistical testing shown are one-way ANOVA with post hoc Tukey's test (liver + kidney) and Kruskal-Wallis test with post hoc Dunn's (spleen).

(C–H) Steady-state plasma concentrations of kynurenine pathway metabolites measured by LC-MS/MS for Kmo^{WT}, Kmo^{null}, and $Kmo^{alb\text{-}cre}$ mouse lines (n = 6 per group). (C) Tryptophan, (D) kynurenine, (E) anthranilic acid, (F) kynurenic acid, (G) 3-hydroxykynurenine, with below limit of quantification (BLQ) threshold 0.09 μM, and (H) xanthurenic acid, with BLQ threshold 0.05 μM. Statistical testings shown are one-way ANOVA (C), pairwise t test comparisons (E, F, and H), or Mann-Whitney test (D, F, and G) against Kmo^{WT}, according to data distribution.

(I–K) Plasma concentrations of tracer compounds and metabolites 20 min after weight-adjusted (50 μg/g) intravenous (i.v.) bolus containing deuterated tryptophan-d_5 (D_5-tryptophan) and $^{13}C_6$-3-hydroxykynurenine ($^{13}C_6$-3HK), measured by LC-MS/MS for Kmo^{WT}, Kmo^{null}, and $Kmo^{alb\text{-}cre}$ mouse lines (n = 6 per group).

(I) D_5-TRP indicates equivalent injection efficiency.

(J) $^{13}C_6$-3HK tracer levels, with BLQ threshold 0.04 μM.

(K) $^{13}C_6$-xanthurenic acid levels. Group statistical testing shown are Kruskal-Wallis test (I) and one-way ANOVA with post hoc Tukey (J and K), according to data distribution.

Plots (C)–(K) show individual data from each mouse, and horizontal lines are median with IQR. ns, not statistically significant ($p > 0.05$); *$p < 0.05$; **$p < 0.01$; ***$p < 0.001$.

(legend on next page)

compared with Kmo^{WT} mice (Figure 1F). Interestingly, and unexpectedly, $Kmo^{alb\text{-}cre}$ mice had high levels of plasma 3-hydroxykynurenine (median 0.8; 0.5 μM 25% percentile and 1.29 μM 75% percentile) compared with Kmo^{WT} mice, in which plasma levels of 3-hydroxykynurenine were below the threshold for detection, which was 0.09 μM (Figure 1G). Elevated 3-hydroxykynurenine in $Kmo^{alb\text{-}cre}$ mice was converted to xanthurenic acid, resulting in a 3-fold increase in plasma xanthurenic acid level compared with Kmo^{WT} mice (median 1.1 vs. 0.4 μM, respectively; p = 0.008, t test) (Figure 1H).

Given the unanticipated finding of elevated plasma 3-hydroxykynurenine in $Kmo^{alb\text{-}cre}$ mice, we examined 3-hydroxykynurenine plasma clearance *in vivo* using stable isotope tracers. A premixed weight-adjusted (50 μg/g body weight) bolus of deuterated tryptophan-indole-d_5 and $^{13}C_6$-3-hydroxykynurenine was injected intravenously into the tail vein of anesthetized $Kmo^{alb\text{-}cre}$ mice, and 20 min later, blood was sampled by cardiac puncture. Injected tracer molecules and their respective tracer metabolites (i.e., kynurenine-d_4 and $^{13}C_6$-xanthurenic acid) were measured together with endogenous kynurenine pathway metabolites in plasma and urine. Equivalent concentrations of tryptophan-indole-d_5 in each mouse line were seen, acting as a dosing control and indicating that tail vein injections were technically successful and comparable (Figure 1I). The plasma level of kynurenine-d_4, the oxidized product of injected d_5-tryptophan, was highest in Kmo^{null} mice, lower in the $Kmo^{alb\text{-}cre}$ line, and lowest in Kmo^{WT} (Figure S1A), consistent with the endogenous metabolite and congruent with the amount of KMO enzyme present in each mouse line. Remarkably, $^{13}C_6$-3-hydroxykynurenine tracer levels in $Kmo^{alb\text{-}cre}$ mice were 10-fold higher compared with Kmo^{WT} mice and 4-fold higher than in Kmo^{null} mice (Figure 1J), and although the $^{13}C_6$-3-hydroxykynurenine tracer could not be detected in the urine of $Kmo^{alb\text{-}cre}$ mice at 20 min after injection, endogenous 3-hydroxykynurenine was detectable and only in $Kmo^{alb\text{-}cre}$ mice compared with the other mouse strains tested (Figures S1B–S1D), thus confirming that urinary excretion is an important mode of elimination of supraphysiological plasma 3-hydroxykynurenine in $Kmo^{alb\text{-}cre}$ mice. Plasma levels of $^{13}C_6$-xanthurenic acid, the transaminated product of injected $^{13}C_6$-3-hydroxykynurenine, were lower in $Kmo^{alb\text{-}cre}$ mice compared with Kmo^{null} mice, likely due to competition for kyneurenine aminotransferase (KAT) enzymes from the elevated endogenous 3-hydroxykynurenine in $Kmo^{alb\text{-}cre}$ mice (Figure 1K).

Taking the endogenous metabolite plasma levels together with the data from the metabolic tracer experiments, it is clear that KMO activity in different tissues results in discrete biochemical phenotypes in that liver KMO is required to be fully functional if low kynurenine plasma concentrations are to be maintained. When liver KMO activity is restricted, kynurenine accumulates in plasma, and that excess is converted to 3-hydroxykynurenine by extra-hepatic KMO. Lastly, elimination of excess circulating 3-hydroxykynurenine from plasma can occur via urinary excretion, and this route is saturable.

$Kmo^{alb\text{-}cre}$ mice with elevated plasma 3-hydroxykynurenine have altered gene transcription of inflammatory immune signaling pathways

Because 3-hydroxykynurenine damages cells when added *in vitro* in cell culture experiments,[11,21] we asked whether elevated 3-hydroxykynurenine levels seen at steady state in $Kmo^{alb\text{-}cre}$ mice constitutively activate a gene transcription injury response. Total RNA sequencing of extracts from snap-frozen whole, non-perfused liver tissue sampled from healthy $Kmo^{alb\text{-}cre}$, Kmo^{WT}, and Kmo^{null} mice (n = 3 male mice per group) revealed complex transcriptional alterations of genes involved in oxidative metabolism and canonical proinflammatory signaling pathways. Statistical analysis showed that $Kmo^{alb\text{-}cre}$ mice had altered expression of genes integral to cytoprotection and immunomodulation, including *Map3k5* (mitogen-activated protein kinase kinase kinase 5), *Cyp3a11* (cytochrome p450 family 3a polypeptide 11), and *Themis* (thymocyte-expressed molecule involved in selection) (Figure 2A, rows 20, 40, and 42, respectively). *Map3k5*, also known as *Ask1* (apoptosis signal-regulating kinase 1), which encodes MAP3K5/ASK1, a conserved intermediate signaling protein important in stress responses, was observed to be significantly downregulated in $Kmo^{alb\text{-}cre}$ mice compared with Kmo^{WT} and Kmo^{null} mice. Deficiency of MAP3K5/ASK1 can increase susceptibility to various cytotoxic stressors.[22] $Kmo^{alb\text{-}cre}$ mice had a marked increase in expression of *Cyp3a11*, a gene that encodes the main catabolism, detoxification, and xenobiotic/drug metabolism cytochrome p450 enzyme.[23] *Themis*, which encodes a T cell-specific protein critically important in T cell development and survival, was markedly upregulated in the $Kmo^{alb\text{-}cre}$ mice.[24] ReactomePA analysis[25] was used to visualize annotated pathways, confirmed biological oxidations, Toll-like receptor (TLR) signaling cascades, cytokine signaling, and cellular stress responses to be significantly altered in $Kmo^{alb\text{-}cre}$ mice compared with Kmo^{null} mice (Figure 2B). Network analysis confirmed statistically significant alterations in inflammatory pathway signaling, as might be predicted given the elevation in plasma 3-hydroxykynurenine (Figure 2C).

Figure 2. Liver tissue transcriptomics and plasma metabolomics at steady state

(A–C) Whole liver tissue RNA sequencing at steady state comparing mouse lines (n = 3 per group).

(A) Heatmap showing the top 50 differentially expressed genes with p <0.05 identified by likelihood ratio tests (DESeq2 in R) with row scaling ((value − mean)/SD) after a log2 transformation between Kmo^{WT}, Kmo^{null}, and $Kmo^{alb\text{-}cre}$.

(B) Paired pathway analysis of differentially expressed genes in liver using a q-value threshold of 0.1 in Reactome software comparing $Kmo^{alb\text{-}cre}$ with Kmo^{null}.

(C) Network map in Reactome of the myeloid differentiating primary response protein (MyD88)-independent TLR4 cascade pathway (R-MMU-166166) in liver tissue comparing $Kmo^{alb\text{-}cre}$ with Kmo^{null}, using a q value <0.001.

(D and E) Plasma metabolomics analysis comparing steady-state Kmo^{WT}, Kmo^{null}, and $Kmo^{alb\text{-}cre}$ mice (n = 6 per group).

(D) Heatmap shows significantly differing metabolites between mouse lines by log fold change compared with mean of all samples using ANOVA with a false discovery rate (FDR)-corrected p <0.05.

(E) Metabolic pathway analysis using MetaboAnalyst and MetaboLights filtered using an FDR of 0.05. Impact values represent the normalized sum of central importance of individual metabolites relative to each pathway as a whole.

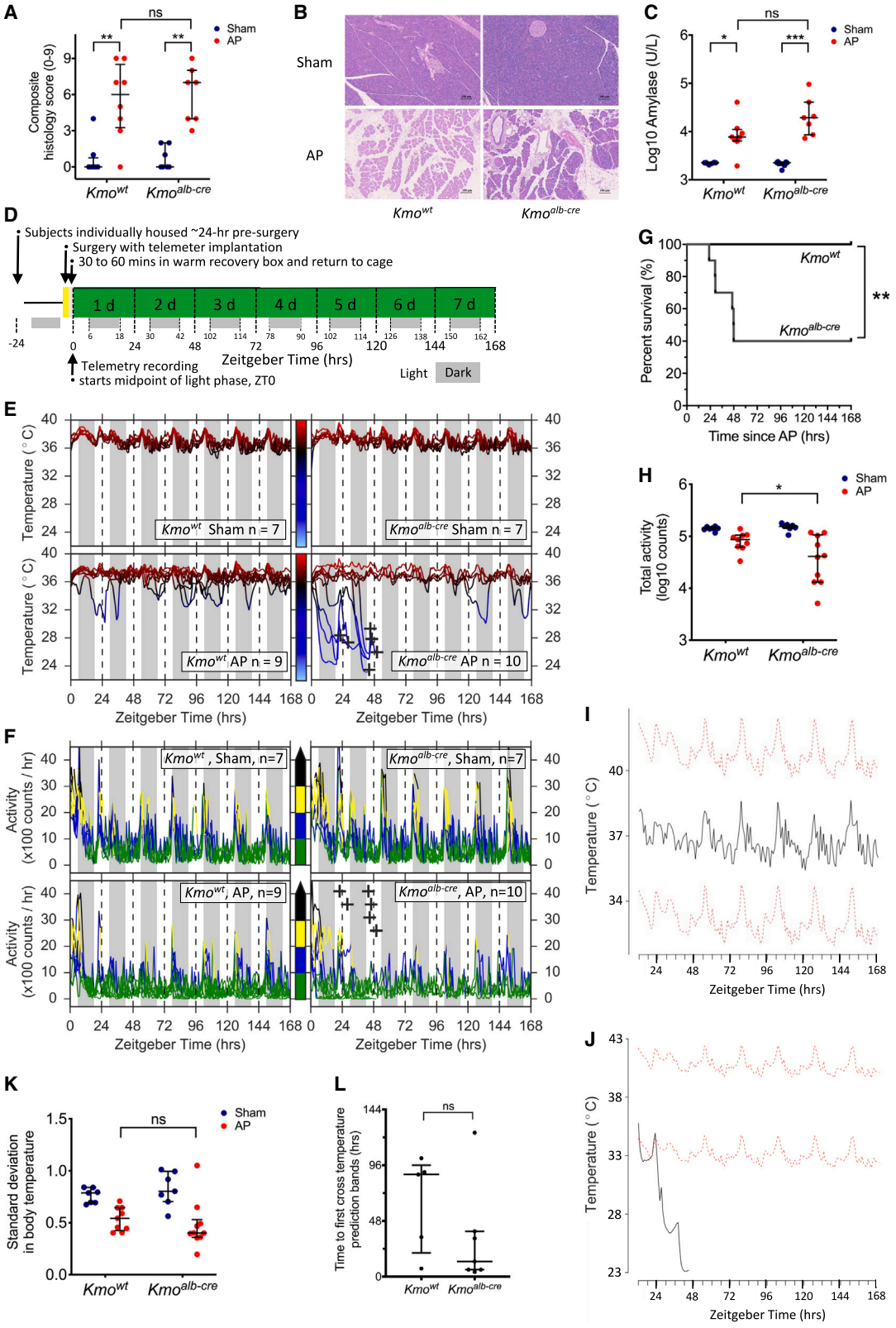

(legend on next page)

None of the observed transcriptomic changes could be accounted for by baseline changes in liver histology. Specifically, liver tissue histological hematoxylin and eosin examination did not show any significant architectural disruption or increased influx of inflammatory cells in $Kmo^{alb\text{-}cre}$ mice compared with Kmo^{WT} and Kmo^{null} mice (Figure S2A). This was corroborated by flow cytometry, with equivalent proportions of Kupffer cells ($CD45^+$, live, $lineage^-$ [CD3′CD19/NK1.1], $Ly6G^-$, Siglec F^-, $CD11b^{lo}$, $F4/80^{hi}$) in single-cell preparations of liver tissue from sham laparotomy control mice from each line ($p = 0.42$, one-way ANOVA) (Figures S2B and S2C). Because of the liver's importance in protein synthesis and fat metabolism, we compared total body weights from available age-matched adult male mice (Figure S2D) and demonstrated that KMO inactivation was inversely related to total body mass. Specifically, Kmo^{null} had the highest body weight (mean 30.3 g, SD 1.8 g), followed by mice with partial *Kmo* knockout, $Kmo^{alb\text{-}cre}$ (29.7 g, SD 1.4 g), and Kmo^{WT} mice, which had the lowest body mass (mean 27.7 g, SD 2.1 g) ($p < 0.001$, one-way ANOVA) (Figure S2E).

Given the remarkable differential gene expression profile in $Kmo^{alb\text{-}cre}$ liver tissue and the central importance of the liver in metabolism, we sought to measure metabolomic differences in plasma, comparing healthy adult $Kmo^{alb\text{-}cre}$ mice with Kmo^{WT} and Kmo^{null} mouse line controls ($n = 5$ mice per group). Kynurenine pathway metabolite levels (i.e., picolinic acid, 3-hydroxykynurenine, quinolinic acid, anthranilic acid, kynurenic acid, kynurenine, and N-acetyl-kynurenine 2 [Figure 2D, rows 1, 9, 10, 18, 19, 20, and 21, respectively]) were altered as expected. S-methylmethionine (Figure 2D, row 14), an activator of Erk1/2 signaling, important in wound healing, was elevated in plasma from Kmo^{null} mice. The statistical impact of the metabolomic alterations between mouse lines was plotted using the software package MetaboLights (Figure 2E), identifying tryptophan metabolism (as anticipated) but also nicotinate and nicotinamide metabolism, in keeping with the feeder role of the kynurenine pathway into NAD^+ metabolism and arachidonic acid metabolism (Figure 2E). Together, these transcriptomic and metabolomic data identify striking alterations in $Kmo^{alb\text{-}cre}$, Kmo^{null}, and Kmo^{WT} mice at steady state that are of central importance to systemic inflammation.

Elevated plasma 3-hydroxykynurenine increases the severity of critical illness in experimental AP

We hypothesized that $Kmo^{alb\text{-}cre}$ mice with elevated 3-hydroxykynurenine levels would have heightened susceptibility to critical illness during experimental AP. To test this, we refined our experimental model of AP to ensure that mice still develop severe AP, but that Kmo^{WT} mice are able to survive and recover, thus allowing room to measure any potential exacerbation of disease severity that might occur in $Kmo^{alb\text{-}cre}$ mice. Furthermore, we wanted to monitor mice under experimental conditions over a longer, more clinically relevant time period in order to study sickness behavior. Induction of experimental AP was performed by an injection of 2% sodium taurocholate in 0.9% saline (by weight/volume) into the pancreatic duct at laparotomy under general anesthetic. First, we validated the induction of AP at 24 h post-injection by histological assessment of fixed sections of pancreas tissue stained with hematoxylin and eosin, scoring the extent of edema, neutrophil infiltrate, and necrosis.[26] At 24 h after induction of AP, there was no significant difference in pancreatic injury score or elevation in serum amylase concentration between $Kmo^{alb\text{-}cre}$ mice and Kmo^{WT} mice (Figures 3A–3C). To measure sickness behavior in experimental AP, we added a minimally invasive telemetry system,

Figure 3. $Kmo^{alb\text{-}cre}$ mice have increased sensitivity to experimental AP over 7 days with tendency toward critical illness

(A–C) Experimental acute pancreatitis (AP) was induced by intraductal infusion of 50 μL 2% Na taurocholate in phosphate-buffered saline (PBS). Kmo^{WT} ($n = 16$) and $Kmo^{alb\text{-}cre}$ ($n = 14$) mice were randomized to AP or sham laparotomy, and pancreas histology (A) and plasma amylase (C) were compared at 24 h.

(A) Composite histological pancreas injury scores.

(B) Representative sections of pancreatic head hematoxylin and eosin stain are shown from mice with scores equal to the median of the group. Normal tissue morphology is seen in sham controls and inflammatory changes of neutrophil cell infiltrate, edema, and acinar necrosis can be seen with AP.

(C) Plasma amylase levels.

Mice in (A) and (C) were the same, and group statistical tests shown are Kruskal-Wallis with post hoc Dunn's.

(D–J) 7 day telemetered AP recovery studies comparing Kmo^{WT} with $Kmo^{alb\text{-}cre}$ mice.

(D) Experimental plan schematic.

(E and F) AP 7 day recovery in Kmo^{WT} and $Kmo^{alb\text{-}cre}$ mouse lines with sham-operated controls. Vertical dark panels are the 12 h dark phase intervals, with light phase in between. Telemetry recording starts half-way through the light phase (Zeitgeber 0 h) <2 h after recovery from anesthesia. A plus symbol (+) indicates time point when a mouse reached a humane endpoint (persistent hypothermia < 26°C, minimal response, or severe labored breathing) and was culled under terminal anesthesia.

(E) Hourly mean core body temperature.

(F) Hourly locomotor activity.

(G) 7 day AP survival curves are shown, with a significantly reduced 7 day survival for $Kmo^{alb\text{-}cre}$ mice compared with Kmo^{WT} by log rank test.

(H) Telemetry analysis revealed a significant reduction in locomotor activity in AP $Kmo^{alb\text{-}cre}$ mice compared with AP Kmo^{WT} by t test.

(I–L) Core body temperature (CBT) analysis. y axis temperatures are individually autoscaled to fit data.

(I) Example CBT trace (black line) of a single $Kmo^{alb\text{-}cre}$ mouse randomized to sham and control prediction bands (dotted red error bars) modeled from Kmo^{WT} sham mice shows recovery within predicted interval.

(J) Example CBT trace (black line) of $Kmo^{alb\text{-}cre}$ littermate randomized to AP with early exit from prediction band interval.

(K) Total CBT SDs for each mouse shows suppression of CBT variability with AP for Kmo^{WT} and $Kmo^{alb\text{-}cre}$ mice but no significant difference between mouse lines by Mann-Whitney test.

(L) The length of time to exit predicted recovery profile band interval is plotted for AP in $Kmo^{alb\text{-}cre}$ and AP in Kmo^{WT} lines, with no significant difference between mouse lines by Mann-Whitney test. In all plots, error bars are median with interquartile range. ns, not significant ($p > 0.05$); *$p < 0.05$; **$p < 0.01$; ***$p < 0.001$.

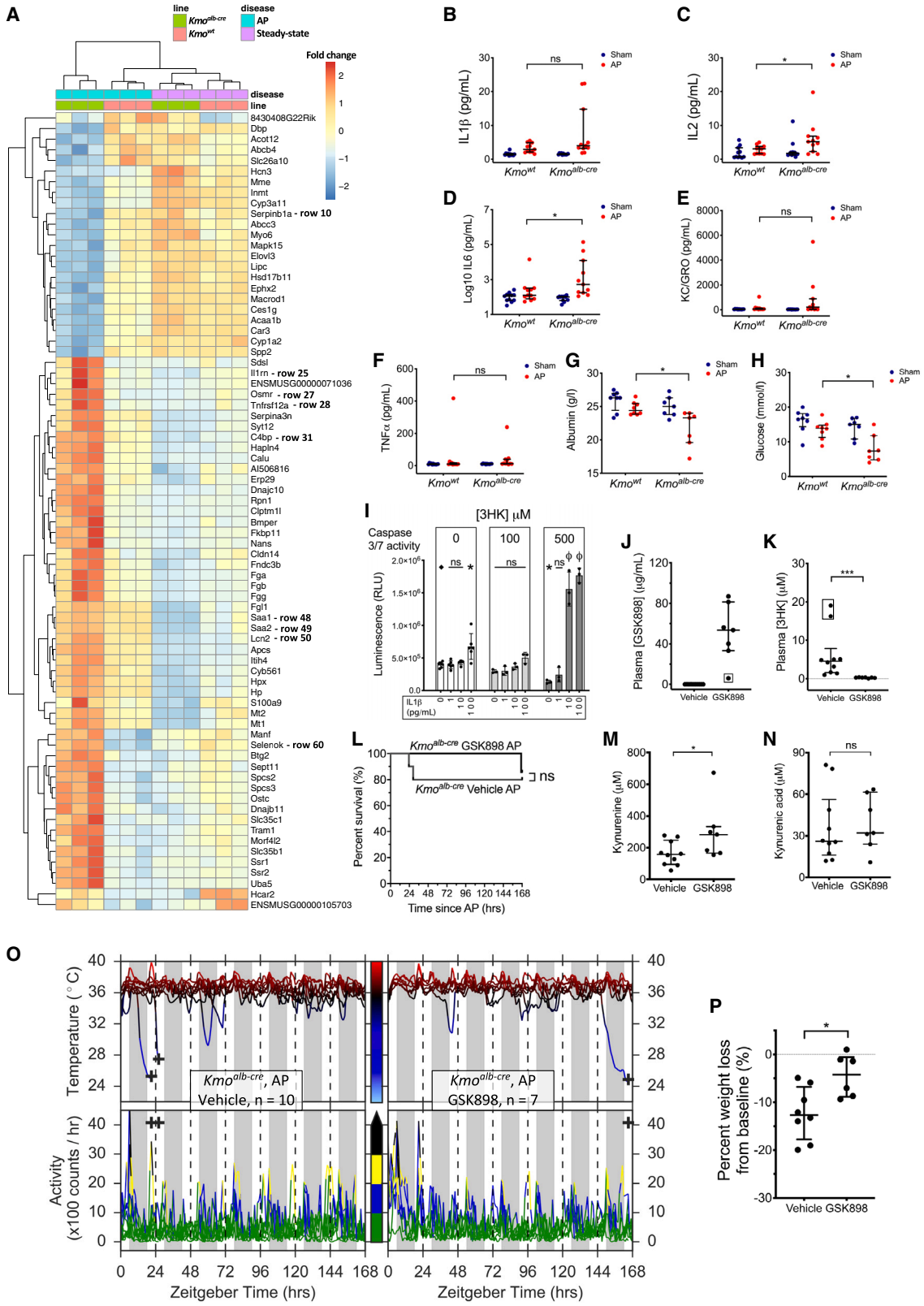

(legend on next page)

which measures locomotor activity and core body temperature, into the protocol when conducting 7 day recovery experiments controlled for light-dark cycles (Figure 3D). In keeping with critical illness, we observed a deregulation of overall homeothermic control and a disrupted circadian locomotor activity in Kmo^{WT} mice and $Kmo^{alb\text{-}cre}$ mice randomized to AP compared with mice from either line randomized to sham operation. Deregulated homeostasis was exacerbated in $Kmo^{alb\text{-}cre}$ mice with AP compared with control Kmo^{WT} mice with AP (Figures 3E and 3F). We had pre-agreed humane endpoints with our veterinarian colleagues, and mice that were euthanized because they had reached those endpoints had biochemical indicators of AP-MODS, specifically elevated serum alanine aminotransferase (ALT; liver injury), elevated serum lactate dehydrogenase (LDH; general cell damage), and elevated serum urea (renal injury) (Figures S3A–S3C). $Kmo^{alb\text{-}cre}$ mice with AP had significantly worse survival than Kmo^{WT} mice with AP ($p = 0.006$, log rank test) (Figure 3G). Analysis of telemetry data revealed a significant ($p = 0.048$, t test) reduction in total locomotor activity in $Kmo^{alb\text{-}cre}$ with AP (median 4.613 log10 total counts; 4.118 25% percentile and 5.027 75% percentile) compared with Kmo^{WT} with AP (median 4.937 log10 total counts; 4.791 25% percentile and 5.021 75% percentile) (Figure 3H).

Statistical analysis of the oscillating telemetry core body temperature data was conducted by first calculating a normal physiological recovery profile using the Kmo^{WT} sham control group to establish prediction bands within which normal recovery data are expected to lie, thresholded with a 0.05 α level. Example traces from individual $Kmo^{alb\text{-}cre}$ mice compared against the Kmo^{WT} sham control prediction bands (dotted red error bars) are shown in Figures 3I and 3J: the top trace (Figure 3I) is the mean hourly core body temperature of a single $Kmo^{alb\text{-}cre}$ mouse randomized to sham laparotomy treatment (black line), and the bottom trace (Figure 3J) is that of a $Kmo^{alb\text{-}cre}$ mouse littermate randomized to AP treatment. Individual mouse tracers with predictions bands are available in Figures S3D and S3E. Collectively, AP reduces variability in core temperature in both mouse lines, resulting in dysregulation of circadian temperature profiles in AP, as indicated by reduced variability (y axis), but the $Kmo^{alb\text{-}cre}$ mouse line has a tendency toward critical illness (Figure 3K). The median experimental time to first drop out (determined from sham Kmo^{WT} recovery profile prediction bands) was less than a sixth of the duration in the $Kmo^{alb\text{-}cre}$ line (13 h, SD 43 h) compared with Kmo^{WT} (88 h, SD 41 h), but with wide variability, the data did not significantly differ between mouse lines ($p = 0.186$, Mann-Whitney test) (Figure 3L).

Elevated plasma 3-hydroxykynurenine exacerbates inflammatory gene transcription during experimental AP

The extent to which 3-hydroxykynurenine levels influence cellular and humoral innate immune responses during systemic inflammation and AP-MODS was unknown. We therefore measured liver tissue RNA sequencing (RNA-seq) transcriptomics from Kmo^{WT} and $Kmo^{alb\text{-}cre}$ mice 24 h after sham operation or induction of experimental AP, where pancreatic injury indices were equivalent between mouse lines in AP and sham (Figures S4A and S4B). For some genes known to be integral to the acute phase response, for example, serum amyloid A1

Figure 4. Effects of AP on gene expression and cytokine profile *in vivo*, synergistic *in vitro* cytotoxicity of IL-1β and 3-hydroxykynurenine, and suppression of early lethality with KMO inhibition in $Kmo^{alb\text{-}cre}$ mice

(A) Heatmap depicts the top 75 genes with significant gene expression from liver tissue of Kmo^{WT} and $Kmo^{alb\text{-}cre}$ mice at 24 h post-AP or -sham (n = 3 per group). Relevant inflammatory genes are highlighted in rows 10 (*Serpinb1a*), 25 (*Il1rn*), 27 (*Osmr*), 28 (*Tnfrsf12a*), 31 (*C4bp*), 48 and 49 (*Saa1* and *Saa2*), 50 (*lipocalin-2* [*Lcn2*]), and 60 (*Selenok*).

(B–F) Plasma cytokine concentrations 24 h post-AP or -sham in Kmo^{WT} and $Kmo^{alb\text{-}cre}$ mice (n = 11 per group, determined by IL-1β power calculation). (B) IL-1β, (C) IL-2, (D) IL-6, (E) KC/GRO, and (F) TNF-α. Statistical pairwise testing shown in (B)–(F) are Mann-Whitney tests. Cytokines IL-1β (B), KC/GRO (E), and TNF-α (F) did not significantly differ between mouse lines in AP, whereas IL-2 (C) and IL-6 (D) were significantly increased in $Kmo^{alb\text{-}cre}$ compared with Kmo^{WT} in AP.

(G and H) Plasma albumin and glucose concentrations at 24 h post-AP or -sham from same mice as in Figures 3A and 3C. Statistical testing shown are t tests.

(G) Albumin levels were significantly lower in $Kmo^{alb\text{-}cre}$ mice compared with Kmo^{WT} in AP.

(H) Glucose levels were significantly lower in $Kmo^{alb\text{-}cre}$ mice compared with Kmo^{WT} in AP.

(I) 3-Hydoxykynurenine (3HK) in co-culture with IL-1β. 3HK at 500 μM potentiated caspase-3/-7 activity with IL-1β (≥10 pg/mL) with a significant elevation in relative luminesce units (RLUs). Groups (n = 3 or 6, as shown) were compared by one-way ANOVA with post hoc Dunnett's test or Kruskal-Wallis with post hoc Dunn's test, according to data distribution. Post hoc tests were made against double blank medium control (◆ 0 μM 3HK and 0 pg/mL IL-1β). Plot (I) shows individual data with horizontal lines as mean and standard error of mean (SEM) error bars.

(J–M) KMO inhibitor drug study in $Kmo^{alb\text{-}cre}$ mice with AP (n = 7 GSK898, n = 10 vehicle).

(J) Log10 concentration of GSK898 drug in plasma determined by LC-MS/MS. The outlier in GSK898 group, marked by a square, denotes a mouse that reached a humane endpoint at 166 h.

(K) Plasma 3HK concentrations at time of cull are shown, and the outliers in vehicle group represent endpoints 24 and 29 h, demonstrating elevated 3HK levels in critical illness. A significant reduction in plasma 3HK levels was observed in $Kmo^{alb\text{-}cre}$ mice with GSK898 treatment, compared with vehicle, by Mann-Whitney test.

(L) 7 day AP survival curves comparing GSK898-treated vs. vehicle-treated $Kmo^{alb\text{-}cre}$ mice with AP, with a log rank test.

(M) Plasma kynurenine concentrations at time of cull.

(N) Plasma kynurenic acid concentrations at time of cull.

(O) Telemetered $Kmo^{alb\text{-}cre}$ mice with AP are shown with CBT (top) and locomotor activity (bottom). A plus symbol (+) indicates a mouse reaching humane endpoint(s) and being culled under terminal anesthesia. Two early deaths (<48 h) were observed in vehicle-treated mice and one death in the GSK898-treated cohort, which occurred much later (167 h).

(P) Percentage weight loss among surviving mice. Vehicle survivors had a median 12% weight loss compared with 4% with GSK898 treatment, a significant reduction by t test. All plots with individual data, except (I), as detailed above, show median with IQR horizontal lines. ns, not significant ($p > 0.05$); *$p < 0.05$; **$p < 0.01$; ***$p < 0.001$; $^{\varphi}p < 0.0001$.

(*Saa1*) and *Saa2*, we observed upregulation of expression in all mice with AP compared with sham operation and to the same extent in both Kmo^{WT} and $Kmo^{alb\text{-}cre}$ mice genotypes (Figure 4A, rows 48 and 49). However, strikingly, and importantly for elucidating how 3-hydroxykynurenine drives inflammation, other key immunomodulatory and proinflammatory genes were profoundly and further increased in $Kmo^{alb\text{-}cre}$ mice with AP compared with Kmo^{WT} with AP, providing valuable mechanistic insight and explaining why $Kmo^{alb\text{-}cre}$ mice have increased AP severity compared with Kmo^{WT} mice during experimental AP-MODS. Notable examples include downregulation of serine peptidase inhibitor clade B member 1a (*Serpinb1a*) (Figure 4A, row 10), upregulation of the anti-inflammatory gene interleukin 1 receptor antagonist (*Il1rn*) (Figure 4A, row 25), upregulation of tumor necrosis factor receptor superfamily member 12 a (*Tnfrsf12a*) (Figure 4A, row 28), and upregulation of C4b-binding protein (*C4bp*) (Figure 4A, row 31), which encodes a major complement regulator, C4bp.

In plasma from $Kmo^{alb\text{-}cre}$ and Kmo^{WT} mice treated with AP or sham, at 24 h, levels of cytokines interleukin-1β ($p = 0.018$, two-way ANOVA, 18% of total variation), interleukin-2 ($p = 0.041$, two-way ANOVA, 8% of total variation), and interleukin-6 ($p < 0.001$, two-way ANOVA, 24% of total variation) were significantly elevated in AP compared with sham across mouse lines. There was a significant isolated rise in $Kmo^{alb\text{-}cre}$ mice with AP compared with sham in keratinocyte chemoattractant/human growth-regulated oncogene (KC/GRO) ($Kmo^{alb\text{-}cre}$ $p < 0.001$, Kmo^{WT} $p = 0.133$; Mann-Whitney tests) and tumor necrosis factor α (TNF-α) ($Kmo^{alb\text{-}cre}$ $p = 0.028$, Kmo^{WT} $p = 0.478$; Mann-Whitney tests), which was not significant in Kmo^{WT} with AP (Figures 4E and 4F). Although the mean and median values were greater in $Kmo^{alb\text{-}cre}$ compared with Kmo^{WT} mice for all cytokines, except for TNF-α in AP, these differences were not statistically significant between mouse lines (Figures 4B–4E). Other proinflammatory cytokines showed no significant changes with AP compared with sham controls: interleukin-4, -5, and -10 and interferon γ (IFNγ) (Figures S4C–S4F). There were significant reductions in plasma albumin and glucose at 24 h with $Kmo^{alb\text{-}cre}$ compared with Kmo^{WT}, consistent with an exaggerated acute phase response (Figures 4G and 4H). There were, however, no significant differences in or biochemical differences in ALT, LDH, or urea between Kmo^{WT} and $Kmo^{alb\text{-}cre}$ in AP (Figures S4G–S4I). Flow cytometric evaluation of myeloid cell subtypes (gating strategies shown in Figures S5A, S5C, and S5K) between Kmo^{WT} and $Kmo^{alb\text{-}cre}$ in AP and sham controls in blood and vital organs showed increased neutrophils in blood and tissues in AP compared with sham ($p = 0.003$, two-way ANOVA) but no significant difference between $Kmo^{alb\text{-}cre}$ and Kmo^{WT} (Figures S5D, S5G, and S5L). Of note, the effect of AP across a kynurenine metabolite panel (tryptophan [TRP], kynurenine [KYN], KA, AA, 3HK, 3HAA, PA, XA) was investigated by comparing metabolite levels at 24 h post-AP ($n = 7$ or 8, per mouse line) compared with sham operation ($n = 7$ or 8, per line) across $Kmo^{alb\text{-}cre}$ and Kmo^{WT} mouse lines. 3-Hydroxykynurenine levels uniquely differed in this sublethal experimental AP model (2% Na-TCA), where a significant increase was detected ($p = 0.042$, two-way ANOVA, 11% of total variation), with a greater magnitude of effect in $Kmo^{alb\text{-}cre}$ observed compared with Kmo^{WT} mice (Figure S6).

Together, these data show that $Kmo^{alb\text{-}cre}$ mice given experimental AP have liver transcriptomic changes that explain the greater severity of AP-MODS associated with elevated plasma 3-hydroxykynurenine.

3-Hydroxykynurenine potentiates interleukin-1β-induced apoptotic caspase activation *in vitro*

Interleukin-1β is integral to systemic inflammation and is elevated in clinical AP in humans and in experimental AP in mice. We therefore asked whether interleukin-1β synergized with 3-hydroxykynurenine to cause cell death in culture. We chose human lung microvascular endothelial cells (HMVEC-Ls) since the most common site for organ dysfunction in AP is the respiratory system, and the endothelial cells are directly exposed to circulating cytokines and kynurenine pathway metabolites. Co-incubation of HMVEC-Ls with 3-hydroxykynurenine (0–500 μM final concentration) and interleukin-1β (0–100 pg/mL final concentration) synergized in activating the core apoptotic pathway components caspase-3 and -7 (Figures 4I and S7A). To substantiate these findings, we measured viability and caspase activation in response to 3-hydroxykynurenine in additional relevant cell types, namely primary human small airway epithelial cells (SAECs) (Figure S8) and the human renal proximal tubule epithelial cell (HRPTEpC) line (Figure S9). In SAECs and HRPTEpCs, caspase activation was uniquely induced by 3-hydroxykynurenine treatment with reduced cell survival in an Alamar blue assay (Figure S8 and S9). In renal tubular HRPTEpCs, 3-hydroxykynurenine and 3-hydroxy-anthranilic acid treatment resulted in a significantly increased caspase-3 and -7 activation (Figure S9A).

Pharmacological KMO inhibition reduces 3-hydroxykynurenine to undetectable levels and rescues $Kmo^{alb\text{-}cre}$ mice from critical illness and excess mortality in experimental AP

Highly selective KMO inhibitors can reduce plasma 3-hydroxykynurenine levels and protect against experimental AP-MODS.[10] Therefore, KMO inhibition has the potential to rescue the critical illness phenotype seen in $Kmo^{alb\text{-}cre}$ mice with AP. To test this, we used a highly selective small-molecule inhibitor of KMO, GSK898, that is a potent inhibitor of KMO activity in human cells (pIC50 8.8 μM), is highly soluble, and has a low volume of distribution (0.31 L/kg) and a moderate half-life (3.6 h).[27] GSK898 in DMSO-PEG-400 solvent, or vehicle, was administered to $Kmo^{alb\text{-}cre}$ mice by continuous subcutaneous infusion with primed osmotic pumps (1002, ALZET, manufactured to deliver 0.25 μL/h drug) implanted into the scruff of mice at a dose of 62.5 μg/h 3 days prior to induction of AP or sham laparotomy and telemeter implantation. Drug levels in plasma were measured by LC-MS/MS and are presented in Figure 4J. GSK898 treatment of $Kmo^{alb\text{-}cre}$ mice reduced plasma 3-hydroxykynurenine concentrations from 4.6 (1.6 μM 25% percentile, 7.9 μM 75% percentile, $n = 10$ mice) to 0.3 μM (0.2 μM 25% percentile, 0.3 μM 75% percentile, $n = 7$ mice) (Figure 4K). GSK898 treatment blockaded extra-hepatic KMO activity, resulting in a further increase in plasma kynurenine (Figure 4M), but this did not result in an additional rise in kynurenic acid, which was already elevated due to the $Kmo^{alb\text{-}cre}$

phenotype (Figure 4N). *Kmo*$^{alb\text{-}cre}$ mice with AP treated with GSK898 were protected from early AP-MODS deaths, and body temperature and locomotor activity telemetry analysis showed less severe sickness behavior (Figures 4L and 4O). Two *Kmo*$^{alb\text{-}cre}$ mice reached the humane endpoint in the vehicle group within 36 h of AP induction compared with one death at 167 h after AP induction in the GSK898 treatment group. *Kmo*$^{alb\text{-}cre}$ mice with AP treated with GSK898 experienced less weight loss than vehicle-treated controls (Figure 4P), indicating better overall health during the experimental period. Cumulatively, these experiments show that systemic pharmacologic KMO inhibition reduces pathological 3-hydroxykynurenine levels and rescues *Kmo*$^{alb\text{-}cre}$ mice from critical illness in experimental AP-MODS.

DISCUSSION

AP-MODS is a manifestation of extreme pathophysiological stress that remains a major unmet medical need. AP-MODS has no disease-modifying treatments available, and patients and their medical teams rely on critical care support of failing organ systems to try and prevent rapid-onset fatality. Despite this, the case fatality rate in AP-MODS remains high.[7] The precise pathological mechanisms that culminate in the sterile systemic inflammatory response syndrome (SIRS), which is the precursor of AP-MODS, are steadily being elucidated, and metabolic flux through KMO is being recognized as an important contributor to the overall pathology of AP-MODS.

Our focus in this work has been on altered metabolism through KMO, the key gatekeeper in the kynurenine pathway of tryptophan metabolism, which is a promising and therapeutically actionable actor in AP,[9] as well as other sterile-MODS diseases including burns,[28] trauma,[29–31] and ischemia-reperfusion injury.[32–34] Flux in kynurenine pathway metabolism is increased during inflammation, initially upregulating tryptophan consumption in the liver by TDO induced by glucocorticoids[35] and elsewhere principally by IDO1. IDO1 is highly induced by IFNs,[36,37] and to a lesser extent by IFN-independent mechanisms, including other proinflammatory mediators, either independently or in synergy with lipopolysaccharide (LPS; e.g., platelet activating factor, interleukin-1β [IL-1β], IL-6, and TNF-α[15,38,39]). However, it is the conversion of kynurenine to the harmful 3-hydroxykynurenine that is the key targetable pathogenic mechanism.

In this article, we generated mice (*Kmo*$^{alb\text{-}cre}$) with genetic knockout of *Kmo* restricted to the hepatocytes of the liver. Unexpectedly, these mice had elevated plasma 3-hydroxykynurenine levels and reduced plasma $^{13}C_6$-3-hydroxykynurenine tracer clearance, which provided an opportunity to measure the effect of elevated 3-hydroxykynurenine during experimental AP and compare those findings with instances where 3-hydroxykynurenine is naturally low, in *Kmo*^{WT} mice, or otherwise repressed by treatment with a highly selective KMO inhibitor. Mice with elevated 3-hydroxykynurenine had transcriptomic alteration of innate immune signaling pathways in liver tissue in unstressed conditions and, when challenged with experimental AP, succumbed fatally earlier and more readily than mice with no blockade of KMO activity. Experimental AP caused elevated plasma IL-1β, and in cells cultured *in vitro*, addition of 3-hydroxykynurenine, but not other kynurenine metabolites, synergized with IL-1β to cause cellular apoptosis. In mice, *in vivo*, giving a highly selective KMO inhibitor to reduce 3-hydroxykynurenine to undetectable levels protected against early critical illness and mortality in experimental AP.

The pathological mechanisms involved in AP-MODS comprise an array of rapid orchestrated host adaptations to tissue and cellular damage, comprising neuroendocrine, immune, cardiovascular, and metabolic changes.[40,41] Early initiators and amplifiers of sterile inflammation and organ failure include the release of DAMPs from injured tissues[42] that are recognized by innate immune receptors (e.g., TLRs, CLRs, NLRs, RAGE), activating intracellular signaling pathways, which induce a "genomic storm."[43] Reprioritized gene expression results in release of proinflammatory mediators that have pleiotropic and multi-systemic effects, including altered metabolism (e.g., aerobic glycolysis), coagulopathy, and dysfunction of leukocytes, the microvasculature, gut defense mechanisms,[44] and mitochondria.[45] Collectively, these responses are generally protective and infer a host survival advantage when they are modest and short lived.

At steady state, KMO acts below its maximum enzymatic rate and has capacity for increased activity with increased kynurenine substrate availability.[46] Although kynurenine pathway enzymes have important functions in the central nervous system, the majority of KMO is expressed in peripheral tissues.[47] *Kmo* gene expression can be induced by innate stimuli such as the TLR4 agonist LPS[14,37] and proinflammatory cytokines IL-1β,[15] TNF-α,[37] and IFNγ.[37] Our lab previously reported that genetic and pharmacologic blockade of KMO protects against experimental AP-MODS in mice and rats.[10] An ever-growing list of KMO inhibitors has been created,[20,48–50] and in particular, certain molecules are actively being evaluated as potential clinical therapeutics to prevent and treat AP-MODS in humans.[27]

An unexpected discovery during this work was finding that when *Kmo* gene knockout is restricted to hepatocytes, as in *Kmo*$^{alb\text{-}cre}$ mice, circulating plasma 3-hydroxykynurenine levels are elevated and have reduced 3-hydroxykynurenine clearance, demonstrating that there is a hepatocyte-restricted role for KMO. KMO is a mitochondria-bound enzyme, and hepatocyte KMO production of 3-hydroxykynureine within the cytoplasm is presumably contained and rapidly catabolized, firstly by kynureninase (plus co-factor vitamin B_6), to form downstream metabolites supplying intermediary metabolism substrates (i.e., total oxidation to form acetyl Co-A, or synthesis *de novo* of NAD^+ cofactor). This depletes plasma stores of kynurenine and thus leaves reduced substrate for extra-hepatic KMO production of 3-hydroxykynurenine. It was no surprise to find elevated concentrations of 3-hydroxykynurenine in the urine of *Kmo*$^{alb\text{-}cre}$ mice since kynurenines were originally discovered in mammalian urine (by J.F. Liebig in 1853) and patients with end-stage renal failure have elevated plasma 3-hydroxykynurenine concentrations.[51] However, it was a noteworthy finding because urine 3-hydroxykynurenine was far greater in the *Kmo*$^{alb\text{-}cre}$ mouse line, confirming that elevated plasma concentrations in these mice was resultant upon increased production of 3-hydroxykynurenine with saturation of the urinary excretory capacity. Importantly, *Kmo*$^{alb\text{-}cre}$ mice had altered inflammatory

gene transcription at baseline steady state, which we attribute to elevated plasma 3-hydroxykynurenine levels.

Altered physiological observations during the SIRS in clinically severe AP typically precedes changes in biochemical blood biomarkers or detectable radiological changes. In preliminary studies, we found that sick mice exhibit hypothermia and reduced physical activity as key signs of illness behavior, and therefore we used an implantable telemeter system to continuously monitor animals throughout 7 day recovery studies. This approach allowed objective identification of premorbid deterioration and chronological insights into sickness behavior and recovery during the experimental time course. Specifically, for those mice that survived but had a significant reduction in body weight, telemetry data were examined for abnormal core temperature and locomotor behaviors. $Kmo^{alb\text{-}cre}$ mice had increased susceptibility to critical illness and organ dysfunction over 7 days compared with control Kmo^{WT} mice with AP despite having equivalent pancreatic damage indices at the 24 h time point.

Given the observed phenotype of impaired recovery in $Kmo^{alb\text{-}cre}$ mice, we suppressed systemic 3-hydroxykynurenine levels using a small-molecule KMO inhibitor, GSK898,[27] to block extra-hepatic KMO activity and revert 3-hydroxykynurenine back to low levels. We avoided the potential confounding factor of poor oral intake after major surgery by using parenteral mini-pumps rather than oral drug-water administration, and by implanting mini-pumps 3 days prior to AP, we ensured a sufficient run-in time for the drug to reduce 3-hydroxykynurenine levels. Importantly, this GSK898 was able to protect $Kmo^{alb\text{-}cre}$ mice from developing early-onset critical illness in the AP model, confirming the key role of this metabolite in critical illness outcomes and reinforcing the rationale for KMO inhibition as a therapeutic strategy to protect against AP-MODS in human AP.

When exposed to the severe inflammatory stress of experimental AP (24 h time point experiment), inflammatory gene upregulation was strongly exaggerated in $Kmo^{alb\text{-}cre}$ mice with AP compared with the more appropriate inflammatory gene upregulation response seen in Kmo^{WT} control mice with AP. This observed alteration in gene expression profile was carried forward into a functional and pathological outcome in that mice with elevated 3-hydroxykynurenine and upregulated inflammatory gene transcription developed worse critical illness and increased mortality when compared with mice with lower levels of 3-hydroxykynurenine.

Liver tissue RNA-seq analysis from steady-state mice with genetically altered kynurenine pathway kinetics revealed an altered inflammatory signature, providing mechanistic insights into why $Kmo^{alb\text{-}cre}$ mice were more susceptible to critical illness during recovery from the major inflammatory insult of experimental AP. Steady-state $Kmo^{alb\text{-}cre}$ mice had marked elevation in expression of genes that encode proteins with roles in lymphocyte activation, detoxification, and innate immunity. $Kmo^{alb\text{-}cre}$ mice had marked downregulation of *Map3k5*, which encodes ASK1, a kinase protein with a key signaling role affecting response to cellular stressors. Importantly, in AP, $Kmo^{alb\text{-}cre}$ mice had marked increased expression of *C4bp*, Selenoprotein K (*Selenok*), oncostatin M receptor (*Osmr*), and *Tnfrsf12a* genes compared with Kmo^{WT} in AP. These genes encode proteins that play important signaling roles in the modulation of complement (Cb4-binding protein), immune activation (selenoprotein K), JAK/STAT signaling cytokine receptor (oncostatin-M-specific receptor subunit β), and both classical and alternative nuclear factor κB (NF-κB) pathways (TWEAK-Fn14), respectively. It is likely that such key changes to the inflammatory profile in $Kmo^{alb\text{-}cre}$ mice correspond with an altered response to AP-induced injury.

3-Hydroxykynurenine is known to induce apoptotic cell death when added to cell cultures *in vitro*.[18,21] One explanation for this effect is the production of cytotoxic levels of reactive oxygen species. Redox-active transition metals (e.g., Cu^{2+} and Fe^{3+}) strongly catalyze the autooxidation of 3-hydroxykynurenine,[52–54] which can thereafter spontaneously form several self-dimerized compounds, including xanthomatin (Xan) and hydroxy-Xan (OH-Xan) and dihydroxy-quinolinone-carboxylic acid (DHQCA).[53–55] During self-dimerization, superoxide, hydrogen peroxide,[55] and hydroxyl radicals[55–58] are generated, which damage DNA,[59] can activate NF-κB,[60] induce apoptosis,[61] cause high intracellular calcium levels,[57,60,62] and release cytochrome *c*.[18] Additionally, 3-hydroxykynurenine can react with and chemically modify cytosolic NAD(P)H oxidase subunits, which promotes translocation of the subunits to the plasma membrane for construction of NAD(P)H oxidase, which can produce superoxide in the process of generating $NADP^+$ from NADPH.[18]

Elimination of 3-hydroxykynurenine is reliant upon excretion or, otherwise, onward metabolism to xanthurenic acid by KATs, or generation of 3-hydroxyanthranilate (3HAA) and L-alanine by kynureninase, which is the major metabolic route.[55] Kynureninase, however, is heavily dependent upon coenzyme vitamin B6, pyridoxal 5′-phosphate (PLP), and is exquisitely sensitive to a lack of this compound, resulting in plasma accumulation of 3-hydroxykynurenine when the supply is insufficient.[63–65] In critical illness, marginal vitamin B6 deficiency is common and likely contributes to elevated plasma 3-hydroxykynurenine levels.[65,66] Indeed, PLP supplementation has been shown to have cytoprotective effects by preventing oxygen radical generation and lipid peroxidation during hydrogen peroxide challenge.[67]

In this article, we additionally showed that 3-hydroxykynurenine can also potentiate apoptotic cell death in primary human vascular endothelial cells in response to IL-1β, a cytokine that is found at increased concentrations in both mouse and human blood in the early stages of AP. IL-1β is made as a procytokine (pro-IL1β), cleaved by protease caspase-1 and secreted by cells of the innate immune system, such as monocytes and macrophages. This may suggest that synergy between 3-hydroxykynurenine and particular cytokines contributes to AP-MODS. Additionally, 3-hydroxykynurenine is known to potentiate the effects of other metabolites, such as quinolinic acid, with cytotoxic effects.[68] From clinical data, it is apparent that patients most at risk of AP-MODS are those with preexisting inflammatory states, specifically smoking, hypertension, diabetes mellitus, and ischemic heart disease.[7] Given that $Kmo^{alb\text{-}cre}$ mice had altered inflammatory gene signatures, we might regard $Kmo^{alb\text{-}cre}$ mice as having preexisting inflammatory gene activation. The protective effect of KMO inhibition in AP indicates additional potential for targeting KMO and evaluating the potential for KMO inhibition in other

situations of excess inflammation, for example in other forms of sterile-MODS.[33]

Limitations of the study

Despite these results showing an important metabolic role for KMO in mouse metabolism that is perturbed by both genetic and small-molecule blockade with profound changes in biochemical phenotype, as yet, data in humans do not yet exist to confirm that KMO blockade results in the same altered biochemical phenotype as shown in Figure 1, and therefore the direct translatability of the findings presented here to human disease remain speculative. As clinical trials of KMO inhibitors progress and human data accrue, greater insight into the potential translatability of KMO inhibition will evolve. By using *Kmo*$^{alb\text{-}cre}$ mice, we were able to eliminate KMO activity in hepatocytes but not in whole liver (that also contains Kuppfer cells, cholangiocytes, and endothelial cells, among other cell types), yet the bulk RNA-seq data were derived from whole liver tissue preparations. Therefore, the interpretation of the RNA-seq data must be made in that context. When considering survival data for all experimental AP groups, because we chose to adopt a humane endpoint as a threshold for cull as a surrogate of mortality (rather than actual mortality), there is always the possibility that some moribund mice could have recovered with time. However, given the clear and objective telemetry data indicating critical illness, this seems unlikely. As with any complex experimental mouse model, especially a surgical model such as that used here, there is an inherent variability in severity; this is exemplified in Figure 4L, where the mortality and the telemetered critical illness behavior in Figure 4P in the untreated group was not as high as that seen in previous iterations of the model and remains unexplained. Together, however, these limitations add nuance to the findings presented here but do not ineffectuate the main results.

In conclusion, our findings establish the KMO product 3-hydroxykynurenine as a key regulator of inflammation and the innate immune response to sterile inflammatory injury. In critical illness, excess morbidity and death from multiple organ failure may be rescued by systemic KMO blockade.

STAR★METHODS

Detailed methods are provided in the online version of this paper and include the following:

- KEY RESOURCES TABLE
- RESOURCE AVAILABILITY
  - Lead contact
  - Materials availability
  - Data and code availability
- EXPERIMENTAL MODEL AND STUDY PARTICIPANT DETAILS
  - Ethical statement
  - Animal welfare and humane endpoints
  - Mice
  - Taurocholate-induced acute pancreatitis
  - Telemetry implantation
- METHOD DETAILS
  - Blood preparation for flow cytometry
  - Tissue preparation for flow cytometry
  - Cell staining and flow cytometry
  - Plasma cytokine assay
  - Clinical biochemical assays
  - Liquid chromatography-tandem mass spectrometry (LC-MS/MS) analysis of tryptophan metabolites
  - Isotope tracer studies
  - Micro-osmotic pump KMOi drug study
  - Pancreas injury histology scoring
  - Gene expression profiling
  - Caspase 3 and 7 activity assays
  - Cell viability assay
- QUANTIFICATION AND STATISTICAL ANALYSIS
  - Telemetry data processing for visualization
  - Telemetry data statistical data analysis
  - RNA-seq data analysis
  - Statistics and power analyses

SUPPLEMENTAL INFORMATION

Supplemental information can be found online at https://doi.org/10.1016/j.celrep.2023.112763.

ACKNOWLEDGMENTS

We wish to thank Dr. Forbes Howie, Shonna Johnson, Dr. William Ramage, and Will Mongall from the University of Edinburgh for their technical assistance. We thank the Named Veterinary Surgeons of the University of Edinburgh for their guidance. We thank Dr. Stuart Hayes of the Anatomically Resolved Dynamics Department, Max Planck Institute for the Structure and Dynamics of Matter, Germany, for training A.J.H. in scientific Python programming for data visualization. A.J.H. and J.O. were funded by the Amelie Waring Fellowship from Guts UK Charity (formerly Core). The University of Edinburgh/GSK have a Discovery Partnership with Academia collaboration. L.P.A.N. holds a Doctoral Training Program PhD studentship from the Medical Research Council. T.B.J.M. was funded by a research bursary from the Royal College of Surgeons of England. J.K.B. is funded by a Wellcome Trust Intermediate Clinical Fellowship (103258/Z/13/Z), a Wellcome-Beit Prize (103258/Z/13/A), a BBSRC Institute Strategic Program Grant to the Roslin Institute, and the UK Intensive Care Society. D.J.M. holds a Senior Clinical Fellowship from the UK Medical Research Council (MR/P008887/1).

AUTHOR CONTRIBUTIONS

Conceptualization, A.J.H. and D.J.M.; methodology, A.J.H., X.Z., T.B.J.M., G.J., N.A.B., and D.J.M.; software, A.J.H. and L.P.A.N.; formal analysis, A.J.H., N.A.B., and D.J.M.; investigation, A.J.H., X.Z., J.O., J.K.B., T.B.J.M., M.B., and G.J.; writing – original draft, A.J.H., I.U., and D.J.M.; writing – review & editing, A.J.H., I.U., K.M., N.A.B., J.K.B., C.S., N.Z.M.H., O.J.G., J.P.I., and D.J.M.; visualization, A.J.H. and L.P.A.N.; project administration, A.J.H. and D.J.M.; resources, A.J.H., X.Z., I.U., J.L., and D.J.M.; supervision, S.E.M.H., J.P.I., and D.J.M.; funding acquisition, A.J.H., O.J.G., J.P.I., and D.J.M.

DECLARATION OF INTERESTS

S.P.W. and D.J.M. are co-founders of Kynos Therapeutics, Ltd. D.J.M. is a board member of Kynos. The University of Edinburgh controls patents WO2015/091647, WO2016/097144, and WO2016/188827, which relate to inhibitors of KMO and include the compound used in this paper.

INCLUSION AND DIVERSITY

We support inclusive, diverse, and equitable conduct of research.

Received: August 10, 2020
Revised: December 14, 2022
Accepted: June 21, 2023

REFERENCES

1. Forsmark, C.E., Baillie, J., and AGA Institute Clinical Practice and Economics Committee; AGA Institute Governing Board; and Board, A.G.A.I.G. (2007). AGA Institute technical review on acute pancreatitis. Gastroenterology *132*, 2022–2044. https://doi.org/10.1053/j.gastro.2007.03.065.

2. Kang, R., Lotze, M.T., Zeh, H.J., Billiar, T.R., and Tang, D. (2014). Cell death and DAMPs in acute pancreatitis. Mol. Med. *20*, 466–477. https://doi.org/10.2119/molmed.2014.00117.

3. Xiao, A.Y., Tan, M.L.Y., Wu, L.M., Asrani, V.M., Windsor, J.A., Yadav, D., and Petrov, M.S. (2016). Global incidence and mortality of pancreatic diseases: a systematic review, meta-analysis, and meta-regression of population-based cohort studies. Lancet. Gastroenterol. Hepatol. *1*, 45–55. https://doi.org/10.1016/S2468-1253(16)30004-8.

4. Peery, A.F., Dellon, E.S., Lund, J., Crockett, S.D., McGowan, C.E., Bulsiewicz, W.J., Gangarosa, L.M., Thiny, M.T., Stizenberg, K., Morgan, D.R., et al. (2012). Burden of gastrointestinal disease in the United States: 2012 update. Gastroenterology *143*, 1179–1187.e3. https://doi.org/10.1053/j.gastro.2012.08.002.

5. Gerasimenko, J.V., Gerasimenko, O.V., and Petersen, O.H. (2014). The role of Ca2+ in the pathophysiology of pancreatitis. J. Physiol. *592*, 269–280. https://doi.org/10.1113/jphysiol.2013.261784.

6. Buter, A., Imrie, C.W., Carter, C.R., Evans, S., and McKay, C.J. (2002). Dynamic nature of early organ dysfunction determines outcome in acute pancreatitis. Br. J. Surg. *89*, 298–302. https://doi.org/10.1046/j.0007-1323.2001.02025.x.

7. Mole, D.J., Gungabissoon, U., Johnston, P., Cochrane, L., Hopkins, L., Wyper, G.M.A., Skouras, C., Dibben, C., Sullivan, F., Morris, A., et al. (2016). Identifying risk factors for progression to critical care admission and death among individuals with acute pancreatitis: a record linkage analysis of Scottish healthcare databases. BMJ Open *6*, e011474. https://doi.org/10.1136/bmjopen-2016-011474.

8. Mole, D.J., Olabi, B., Robinson, V., Garden, O.J., and Parks, R.W. (2009). Incidence of individual organ dysfunction in fatal acute pancreatitis: analysis of 1024 death records. HPB *11*, 166–170. https://doi.org/10.1111/j.1477-2574.2009.00038.x.

9. Skouras, C., Zheng, X., Binnie, M., Homer, N.Z.M., Murray, T.B.J., Robertson, D., Briody, L., Paterson, F., Spence, H., Derr, L., et al. (2016). Increased levels of 3-hydroxykynurenine parallel disease severity in human acute pancreatitis. Sci. Rep. *6*, 33951. https://doi.org/10.1038/srep33951.

10. Mole, D.J., Webster, S.P., Uings, I., Zheng, X., Binnie, M., Wilson, K., Hutchinson, J.P., Mirguet, O., Walker, A., Beaufils, B., et al. (2016). Kynurenine-3-monooxygenase inhibition prevents multiple organ failure in rodent models of acute pancreatitis. Nat. Med. *22*, 202–209. https://doi.org/10.1038/nm.4020.

11. Mole, D.J., McFerran, N.V., Collett, G., O'Neill, C., Diamond, T., Garden, O.J., Kylanpaa, L., Repo, H., and Deitch, E.A. (2008). Tryptophan catabolites in mesenteric lymph may contribute to pancreatitis-associated organ failure. Br. J. Surg. *95*, 855–867. https://doi.org/10.1002/bjs.6112.

12. Cervenka, I., Agudelo, L.Z., and Ruas, J.L. (2017). Kynurenines: Tryptophan's metabolites in exercise, inflammation, and mental health. Science *357*, eaaf9794. https://doi.org/10.1126/science.aaf9794.

13. Badawy, A.A.B. (2002). Tryptophan metabolism in alcoholism. Nutr. Res. Rev. *15*, 123–152. https://doi.org/10.1079/NRR200133.

14. Connor, T.J., Starr, N., O'Sullivan, J.B., and Harkin, A. (2008). Induction of indolamine 2,3-dioxygenase and kynurenine 3-monooxygenase in rat brain following a systemic inflammatory challenge: a role for IFN-gamma? Neurosci. Lett. *441*, 29–34. https://doi.org/10.1016/j.neulet.2008.06.007.

15. Zunszain, P.A., Anacker, C., Cattaneo, A., Choudhury, S., Musaelyan, K., Myint, A.M., Thuret, S., Price, J., and Pariante, C.M. (2012). Interleukin-1beta: a new regulator of the kynurenine pathway affecting human hippocampal neurogenesis. Neuropsychopharmacology *37*, 939–949. https://doi.org/10.1038/npp.2011.277.

16. Alberati-Giani, D., Ricciardi-Castagnoli, P., Köhler, C., and Cesura, A.M. (1996). Regulation of the kynurenine metabolic pathway by interferon-gamma in murine cloned macrophages and microglial cells. J. Neurochem. *66*, 996–1004.

17. Mizdrak, J., Hains, P.G., Truscott, R.J.W., Jamie, J.F., and Davies, M.J. (2008). Tryptophan-derived ultraviolet filter compounds covalently bound to lens proteins are photosensitizers of oxidative damage. Free Radic. Biol. Med. *44*, 1108–1119. https://doi.org/10.1016/j.freeradbiomed.2007.12.003.

18. Wang, Q., Zhang, M., Ding, Y., Wang, Q., Zhang, W., Song, P., and Zou, M.H. (2014). Activation of NAD(P)H oxidase by tryptophan-derived 3-hydroxykynurenine accelerates endothelial apoptosis and dysfunction in vivo. Circ. Res. *114*, 480–492. https://doi.org/10.1161/CIRCRESAHA.114.302113.

19. Hutchinson, J.P., Rowland, P., Taylor, M.R.D., Christodoulou, E.M., Haslam, C., Hobbs, C.I., Holmes, D.S., Homes, P., Liddle, J., Mole, D.J., et al. (2017). Structural and mechanistic basis of differentiated inhibitors of the acute pancreatitis target kynurenine-3-monooxygenase. Nat. Commun. *8*, 15827. https://doi.org/10.1038/ncomms15827.

20. Liddle, J., Beaufils, B., Binnie, M., Bouillot, A., Denis, A.A., Hann, M.M., Haslam, C.P., Holmes, D.S., Hutchinson, J.P., Kranz, M., et al. (2017). The discovery of potent and selective kynurenine 3-monooxygenase inhibitors for the treatment of acute pancreatitis. Bioorg. Med. Chem. Lett. *27*, 2023–2028. https://doi.org/10.1016/j.bmcl.2017.02.078.

21. Wilson, K., Auer, M., Binnie, M., Zheng, X., Pham, N.T., Iredale, J.P., Webster, S.P., and Mole, D.J. (2016). Overexpression of human kynurenine-3-monooxygenase protects against 3-hydroxykynurenine-mediated apoptosis through bidirectional nonlinear feedback. Cell Death Dis. *7*, e2197. https://doi.org/10.1038/cddis.2016.87.

22. Takeda, K., Noguchi, T., Naguro, I., and Ichijo, H. (2008). Apoptosis signal-regulating kinase 1 in stress and immune response. Annu. Rev. Pharmacol. Toxicol. *48*, 199–225. https://doi.org/10.1146/annurev.pharmtox.48.113006.094606.

23. Anzenbacher, P., and Anzenbacherová, E. (2001). Cytochromes P450 and metabolism of xenobiotics. Cell. Mol. Life Sci. *58*, 737–747.

24. Choi, S., Warzecha, C., Zvezdova, E., Lee, J., Argenty, J., Lesourne, R., Aravind, L., and Love, P.E. (2017). THEMIS enhances TCR signaling and enables positive selection by selective inhibition of the phosphatase SHP-1. Nat. Immunol. *18*, 433–441. https://doi.org/10.1038/ni.3692.

25. Yu, G., and He, Q.Y. (2016). ReactomePA: an R/Bioconductor package for reactome pathway analysis and visualization. Mol. Biosyst. *12*, 477–479. https://doi.org/10.1039/c5mb00663e.

26. Van Laethem, J.L., Marchant, A., Delvaux, A., Goldman, M., Robberecht, P., Velu, T., and Devière, J. (1995). Interleukin 10 prevents necrosis in murine experimental acute pancreatitis. Gastroenterology *108*, 1917–1922.

27. Walker, A.L., Ancellin, N., Beaufils, B., Bergeal, M., Binnie, M., Bouillot, A., Clapham, D., Denis, A., Haslam, C.P., Holmes, D.S., et al. (2017). Development of a series of kynurenine 3-monooxygenase inhibitors leading to a clinical candidate for the treatment of acute Pancreatitis. J. Med. Chem. *60*, 3383–3404. https://doi.org/10.1021/acs.jmedchem.7b00055.

28. Barlow, G.B., and Wilkinson, A.W. (1972). The effect of burns on the metabolism of tryptophan in children. Clin. Chim. Acta *41*, 169–174. https://doi.org/10.1016/0009-8981(72)90508-6.

29. Lögters, T.T., Laryea, M.D., Altrichter, J., Sokolowski, J., Cinatl, J., Reipen, J., Linhart, W., Windolf, J., Scholz, M., and Wild, M. (2009). Increased plasma kynurenine values and kynurenine-tryptophan ratios after major trauma are early indicators for the development of sepsis. Shock *32*, 29–34.

30. Pellegrin, K., Neurauter, G., Wirleitner, B., Fleming, A.W., Peterson, V.M., and Fuchs, D. (2005). Enhanced enzymatic degradation of tryptophan by indoleamine 2,3-dioxygenase contributes to the tryptophan-deficient state seen after major trauma. Shock *23*, 209–215.

31. Ploder, M., Spittler, A., Kurz, K., Neurauter, G., Pelinka, L.E., Roth, E., and Fuchs, D. (2010). Accelerated tryptophan degradation predicts poor survival in trauma and sepsis patients. Int. J. Tryptophan Res. *3*, 61–67. https://doi.org/10.4137/ijtr.s3983.

32. Bakhta, O., Pascaud, A., Dieu, X., Beaumont, J., Kouassi Nzoughet, J., Kamel, R., Croyal, M., Tamareille, S., Simard, G., Chao de la Barca, J.M., et al. (2020). Tryptophane-kynurenine pathway in the remote ischemic conditioning mechanism. Basic Res. Cardiol. *115*, 13. https://doi.org/10.1007/s00395-019-0770-x.

33. Zheng, X., Zhang, A., Binnie, M., McGuire, K., Webster, S.P., Hughes, J., Howie, S.E.M., and Mole, D.J. (2019). Kynurenine 3-monooxygenase is a critical regulator of renal ischemia-reperfusion injury. Exp. Mol. Med. *51*, 1–14. https://doi.org/10.1038/s12276-019-0210-x.

34. Mohib, K., Wang, S., Guan, Q., Mellor, A.L., Sun, H., Du, C., and Jevnikar, A.M. (2008). Indoleamine 2,3-dioxygenase expression promotes renal ischemia-reperfusion injury. Am. J. Physiol. Renal Physiol. *295*, F226–F234. https://doi.org/10.1152/ajprenal.00567.2007.

35. Nakamura, T., Shinno, H., and Ichihara, A. (1980). Insulin and glucagon as a new regulator system for tryptophan oxygenase activity demonstrated in primary cultured rat hepatocytes. J. Biol. Chem. *255*, 7533–7535.

36. Ozaki, Y., Edelstein, M.P., and Duch, D.S. (1987). The actions of interferon and antiinflammatory agents of induction of indoleamine 2,3-dioxygenase in human peripheral blood monocytes. Biochem. Biophys. Res. Commun. *144*, 1147–1153. https://doi.org/10.1016/0006-291x(87)91431-8.

37. Chiarugi, A., Calvani, M., Meli, E., Traggiai, E., and Moroni, F. (2001). Synthesis and release of neurotoxic kynurenine metabolites by human monocyte-derived macrophages. J. Neuroimmunol. *120*, 190–198. https://doi.org/10.1016/s0165-5728(01)00418-0.

38. Smith, D.G., Guillemin, G.J., Pemberton, L., Kerr, S., Nath, A., Smythe, G.A., and Brew, B.J. (2001). Quinolinic acid is produced by macrophages stimulated by platelet activating factor, Nef and Tat. J. Neurovirol. *7*, 56–60. https://doi.org/10.1080/135502801300069692.

39. Fujigaki, H., Saito, K., Fujigaki, S., Takemura, M., Sudo, K., Ishiguro, H., and Seishima, M. (2006). The signal transducer and activator of transcription 1alpha and interferon regulatory factor 1 are not essential for the induction of indoleamine 2,3-dioxygenase by lipopolysaccharide: involvement of p38 mitogen-activated protein kinase and nuclear factor-kappaB pathways, and synergistic effect of several proinflammatory cytokines. J. Biochem. *139*, 655–662. https://doi.org/10.1093/jb/mvj072.

40. Cuthbertson, D.P., Angeles Valero Zanuy, M.A., and León Sanz, M.L. (2001). Post-shock metabolic response. Nutr. Hosp. *16*, 176–182. discussion 175-176.

41. Cuthbertson, D. (1970). Intensive-care-metabolic response to injury. Br. J. Surg. *57*, 718–721. https://doi.org/10.1002/bjs.1800571003.

42. Eppensteiner, J., Davis, R.P., Barbas, A.S., Kwun, J., and Lee, J. (2018). Immunothrombotic activity of damage-associated molecular patterns and extracellular vesicles in secondary organ failure induced by trauma and sterile insults. Front. Immunol. *9*, 190. https://doi.org/10.3389/fimmu.2018.00190.

43. Xiao, W., Mindrinos, M.N., Seok, J., Cuschieri, J., Cuenca, A.G., Gao, H., Hayden, D.L., Hennessy, L., Moore, E.E., Minei, J.P., et al. (2011). A genomic storm in critically injured humans. J. Exp. Med. *208*, 2581–2590. https://doi.org/10.1084/jem.20111354.

44. Mittal, R., and Coopersmith, C.M. (2014). Redefining the gut as the motor of critical illness. Trends Mol. Med. *20*, 214–223. https://doi.org/10.1016/j.molmed.2013.08.004.

45. Singer, M. (2017). Critical illness and flat batteries. Crit. Care *21*, 309. https://doi.org/10.1186/s13054-017-1913-9.

46. Bender, D.A., and McCreanor, G.M. (1982). The preferred route of kynurenine metabolism in the rat. Biochim. Biophys. Acta *717*, 56–60. https://doi.org/10.1016/0304-4165(82)90379-8.

47. Wonodi, I., and Schwarcz, R. (2010). Cortical kynurenine pathway metabolism: a novel target for cognitive enhancement in Schizophrenia. Schizophr. Bull. *36*, 211–218. https://doi.org/10.1093/schbul/sbq002.

48. Amaral, M., Levy, C., Heyes, D.J., Lafite, P., Outeiro, T.F., Giorgini, F., Leys, D., and Scrutton, N.S. (2013). Structural basis of kynurenine 3-monooxygenase inhibition. Nature *496*, 382–385. https://doi.org/10.1038/nature12039.

49. Smith, J.R., Jamie, J.F., and Guillemin, G.J. (2016). Kynurenine-3-monooxygenase: a review of structure, mechanism, and inhibitors. Drug Discov. Today *21*, 315–324. https://doi.org/10.1016/j.drudis.2015.11.001.

50. Schwarcz, R., and Pellicciari, R. (2002). Manipulation of brain kynurenines: glial targets, neuronal effects, and clinical opportunities. J. Pharmacol. Exp. Ther. *303*, 1–10. https://doi.org/10.1124/jpet.102.034439.

51. Pawlak, K., Domaniewski, T., Mysliwiec, M., and Pawlak, D. (2009). The kynurenines are associated with oxidative stress, inflammation and the prevalence of cardiovascular disease in patients with end-stage renal disease. Atherosclerosis *204*, 309–314. https://doi.org/10.1016/j.atherosclerosis.2008.08.014.

52. Goldstein, L.E., Leopold, M.C., Huang, X., Atwood, C.S., Saunders, A.J., Hartshorn, M., Lim, J.T., Faget, K.Y., Muffat, J.A., Scarpa, R.C., et al. (2000). 3-Hydroxykynurenine and 3-hydroxyanthranilic acid generate hydrogen peroxide and promote alpha-crystallin cross-linking by metal ion reduction. Biochemistry *39*, 7266–7275.

53. Ishii, T., Iwahashi, H., Sugata, R., and Kido, R. (1992). Formation of hydroxanthommatin-derived radical in the oxidation of 3-hydroxykynurenine. Arch. Biochem. Biophys. *294*, 616–622.

54. Vazquez, S., Garner, B., Sheil, M.M., and Truscott, R.J. (2000). Characterisation of the major autoxidation products of 3-hydroxykynurenine under physiological conditions. Free Radic. Res. *32*, 11–23.

55. Zhuravlev, A.V., Vetrovoy, O.V., and Savvateeva-Popova, E.V. (2018). Enzymatic and non-enzymatic pathways of kynurenines' dimerization: the molecular factors for oxidative stress development. PLoS Comput. Biol. *14*, e1006672. https://doi.org/10.1371/journal.pcbi.1006672.

56. Okuda, S., Nishiyama, N., Saito, H., and Katsuki, H. (1996). Hydrogen peroxide-mediated neuronal cell death induced by an endogenous neurotoxin, 3-hydroxykynurenine. Proc. Natl. Acad. Sci. USA *93*, 12553–12558.

57. Wei, H., Leeds, P., Chen, R.W., Wei, W., Leng, Y., Bredesen, D.E., and Chuang, D.M. (2000). Neuronal apoptosis induced by pharmacological concentrations of 3-hydroxykynurenine: characterization and protection by dantrolene and Bcl-2 overexpression. J. Neurochem. *75*, 81–90.

58. Eastman, C.L., and Guilarte, T.R. (1989). Cytotoxicity of 3-hydroxykynurenine in a neuronal hybrid cell line. Brain Res. *495*, 225–231.

59. Hiraku, Y., Inoue, S., Oikawa, S., Yamamoto, K., Tada, S., Nishino, K., and Kawanishi, S. (1995). Metal-mediated oxidative damage to cellular and isolated DNA by certain tryptophan metabolites. Carcinogenesis *16*, 349–356.

60. Schmidt, K.N., Amstad, P., Cerutti, P., and Baeuerle, P.A. (1995). The roles of hydrogen peroxide and superoxide as messengers in the activation of transcription factor NF-kappa B. Chem. Biol. *2*, 13–22.

61. Whittemore, E.R., Loo, D.T., Watt, J.A., and Cotman, C.W. (1995). A detailed analysis of hydrogen peroxide-induced cell death in primary neuronal culture. Neuroscience *67*, 921–932.

62. Distelhorst, C.W., Lam, M., and McCormick, T.S. (1996). Bcl-2 inhibits hydrogen peroxide-induced ER Ca2+ pool depletion. Oncogene *12*, 2051–2055.

63. Guilarte, T.R., and Wagner, H.N., Jr. (1987). Increased concentrations of 3-hydroxykynurenine in vitamin B6 deficient neonatal rat brain. J. Neurochem. *49*, 1918–1926. https://doi.org/10.1111/j.1471-4159.1987.tb02455.x.

64. Theofylaktopoulou, D., Ulvik, A., Midttun, Ø., Ueland, P.M., Vollset, S.E., Nygård, O., Hustad, S., Tell, G.S., and Eussen, S.J.P.M. (2014). Vitamins B2 and B6 as determinants of kynurenines and related markers of interferon-gamma-mediated immune activation in the community-based Hordaland Health Study. Br. J. Nutr. *112*, 1065–1072. https://doi.org/10.1017/S0007114514001858.

65. Midttun, O., Ulvik, A., Ringdal Pedersen, E., Ebbing, M., Bleie, O., Schartum-Hansen, H., Nilsen, R.M., Nygård, O., and Ueland, P.M. (2011). Low plasma vitamin B-6 status affects metabolism through the kynurenine pathway in cardiovascular patients with systemic inflammation. J. Nutr. *141*, 611–617. https://doi.org/10.3945/jn.110.133082.

66. Hou, C.T., Wu, Y.H., Huang, P.N., Cheng, C.H., and Huang, Y.C. (2011). Higher plasma pyridoxal 5'-phosphate is associated with better blood glucose responses in critically ill surgical patients with inadequate vitamin B-6 status. Clin. Nutr. *30*, 478–483. https://doi.org/10.1016/j.clnu.2011.01.014.

67. Kannan, K., and Jain, S.K. (2004). Effect of vitamin B6 on oxygen radicals, mitochondrial membrane potential, and lipid peroxidation in H2O2-treated U937 monocytes. Free Radic. Biol. Med. *36*, 423–428. https://doi.org/10.1016/j.freeradbiomed.2003.09.012.

68. Guidetti, P., and Schwarcz, R. (1999). 3-Hydroxykynurenine potentiates quinolinate but not NMDA toxicity in the rat striatum. Eur. J. Neurosci. *11*, 3857–3863. https://doi.org/10.1046/j.1460-9568.1999.00806.x.

69. Xia, J., Sinelnikov, I.V., Han, B., and Wishart, D.S. (2015). MetaboAnalyst 3.0–making metabolomics more meaningful. Nucleic Acids Res. *43*, W251–W257. https://doi.org/10.1093/nar/gkv380.

STAR★METHODS

KEY RESOURCES TABLE

REAGENT or RESOURCE	SOURCE	IDENTIFIER
Antibodies		
CD16/CD32 mouse BD Fc Block	BD Biosciences	RRID:AB_394657; #553142
CD3-PE clone 17A2	BioLegend	RRID:AB_312662; #100205
CD11B-BV421 clone M1/70	BioLegend	RRID:AB_11203704; #101236
CD11C-PE-Cy7 clone N418	BioLegend	RRID:AB_493568; #117318
CD19-PE clone 6D5	BioLegend	RRID:AB_313643; #115508
CD45-AF700 clone 30-F11	BioLegend	RRID:AB_493715; #103128
CD64-APC clone FcγRI	BioLegend	RRID:AB_11219391; #139306
CD115-APC clone: CSF-1R	BioLegend	RRID:AB_2085221; #135510
F4/80-APC clone CI:A3-1	AbD Serotec	RRID:AB_2098197; #MCA497APCT
Ly6C-FITC clone HK1.4	BioLegend	RRID:AB_1186135; #128006
Ly6G-PerCP/Cy5.5 clone 1A8	BioLegend	RRID:AB_1877271; #127616
MHCII-APC/Fire™ 750 clone I-A/I-E	BioLegend	RRID:AB_2616729; #107652
NK1.1-PE clone PK136	BioLegend	RRID:AB_313395; #108708
Siglec-F-PE-CF594 clone E50-2440	BD Bioscience	RRID:AB_2687994; #562757
Chemicals, peptides, and recombinant proteins		
Taurocholic acid sodium salt hydrate	Sigma	Cat. T4009
Fixable Viability Dye eFluro 455 UV	Thermo/eBioscience	65-0868-14
Human interleukin-1β	Miltenyi Biotec	130-093-895
Human interleukin-6	Miltenyi Biotec	130-095-365
Human interleukin-10	Miltenyi Biotec	130-093-947
Critical commercial assays		
Mouse lung dissociation kit	Miltenyi Biosciences	#130-095-927
Mouse liver dissociation kit	Miltenyi Biosciences	#130-105-807
V-PLEX Proinflammatory Panel1 mouse cytokine kits	Meso Scale Discovery	K15048D-1
Deposited data		
RNASeq data files	BioStudies ArrayExpress	Accession: E-MTAB-13049
Experimental models: Cell lines		
Human Lung Microvascular Endothelial Cells (HMVEC-L)	Lonza	#CC-2527
Human Small Airway Epithelial Cells (SAEC)	Lonza	#CC-2547
EGM™ Endothelial Cell Growth Medium BulletKit™	Lonza	#CC-3124
SAGM™ Small Airway Epithelial Cell Growth Medium BulletKit™	Lonza	#CC-3118
Human renal proximal tubule epithelial cells (HRPTEpC)	Sigma	#930-05A
RenaEpi Growth Medium	Sigma	#911-500
Experimental models: Organisms/strains		
Albumin-Cre mice - B6.Cg-Speer6-ps1Tg(Alb-cre)21Mgn/J	Jackson Laboratories	RRID:IMSR_JAX:003574
Floxed KMO mice - Kmotm1a(KOMP)Wtsi	Our colony	Ref. 10
FLP Deleter - C57BL/6-Tg(CAG-Flpe)2Arte	Taconic Inc.	Cat. 7089-M
Oligonucleotides		
LacZ, forward, 5-GAGTTGCGTGACTACCTACGG- 3′	Sigma	Custom order
LacZ, reverse, 5′-GTACCACAGCGGATGGTTCGG-3′	Sigma	Custom order
Kmo, forward, 5′-GCATTAAAGGACAGTCAACCTG-3′	Sigma	Custom order
Kmo, reverse, 5′-CACTGGACTGT GAGTGCTTG-3′	Sigma	Custom order
Alb-cre forward, 5′-GCGGTCTGGCAGTAAAAACTATC-3′	Sigma	Custom order
Alb-cre reverse, 5′-GTGAAACAGCATTGCTGTCACTT-3′	Sigma	Custom order
TaqMan KMO real-time PCR probe	Thermo	Mm01321344_m1

(*Continued on next page*)

Continued

REAGENT or RESOURCE	SOURCE	IDENTIFIER
Software and algorithms		
VitalView 5.1	Starr Life Sciences	Vital View 5.1
Telemetry processing algorithm	Deposited on Github	https://github.com/HayesAJ83/HayesMole_CellRep.git
FlowJo software V10.1r5	Tree Star	V10.1r5
Other		
Rodent diet RM1	SDS Diets	SDS RM1
Telemetry transmitter G2-E-mitter	Starr Life Sciences	G2EM
Telemetry Energizer/receiver	Starr Life Sciences	ER-4000
EDTA tubes (Microvette®)	Sarstedt	CB 300 K2E
ACE C18-PFP column; 100 × 2.1 mm int. diam 1.7 μm	Waters	ACE C18-PFP

RESOURCE AVAILABILITY

Lead contact

Further information and requests for resources and reagents should be directed to and will be fulfilled by the lead contact, Damian Mole (damian.mole@ed.ac.uk).

Materials availability

Mouse lines used in this study are either commercially available as listed in the key resources table or available from the lead contact on request. All other materials and reagents are commercially available.

Data and code availability

Original code for the telemetry analysis has been deposited at GitHub (provided in the key resources table) and is publicly available. RNA-seq data have been deposited at BioStudies Array Express (www.ebi.ac.uk) and will be made publicly available as of the date of publication. The accession number is ArrayExpress: E-MTAB-13049 and is listed in the key resources table. Any additional information required to reanalyze the data reported in this paper is available from the lead contact upon request.

EXPERIMENTAL MODEL AND STUDY PARTICIPANT DETAILS

Ethical statement

All experiments involving the use of animals were conducted in accordance with the Animals (Scientific Procedures) Act, 1986 governed by the UK Government Home Office, and after review from The University of Edinburgh research ethics committee and veterinary services. Humane cull experimental endpoints were predefined and agreed with the Named Veterinary Surgeon.

Animal welfare and humane endpoints

To test our hypothesis concerning the occurrence of critical illness over a 7-day time course, we prospectively defined critical illness humane endpoints as well as criteria for analgesia in consultation with veterinarians. Endpoints indicating imminent death were unresponsiveness, severe labored breathing and sustained profound hypothermia. Core body temperature was measured by implanted telemetry. Mice were euthanised by exsanguination under deep inhalational anesthesia using isoflurane gas in oxygen. Criteria for euthanasia in a critically ill animal consisted of persistent and profound hypothermia (telemetered core body temperature below 26°C), minimal response to gentle stimulation, or severe labored breathing. Mice found to be hypothermic (defined as 26 to 30°C) underwent a single resuscitation attempt, which consisted of 30-min in a warming chamber (heated box at 30°C) and administered a 0.5 mL warmed subcutaneous fluid bolus (5% dextrose-Dulbecco's PBS wt/vol). All mice were given pre-emptive analgesia whilst under general anesthesia immediately before laparotomy with subcutaneous buprenorphine (0.05 mg/kg body weight, in 5% dextrose-DPBS wt/vol), and a further two doses (6–8 h and 20–24 h post-operatively). Additional doses of subcutaneous buprenorphine were given in accordance with prospectively defined criteria outlined in the cage-side clinical observation score sheet. In anticipation of pain throughout the 7-day period, a daily supply of oral buprenorphine (0.01 mg) was provided in 0.5 mL jelly doses.

Mice

Throughout this study, adult male mice (>16 weeks old) were investigated. Three genetically altered mouse lines on a C57BL/6J background have been generated by our group to study the effect of kynurenine 3-monooxygenase (*Kmo*) gene inactivation. These separate mouse lines were originally derived from embryonic stem cells engineered by the International Knockout Mouse Project (iKOMP), using a 'knockout-first' approach, which has been described in detail previously.[10] Briefly, a global *Kmo*-deleted mouse line (referred to as Kmo^{null}) was first engineered with FRT restriction sites flanking a transcription stop signal in exon 3 of the *Kmo* gene and *loxP* sites flanking key *Kmo* gene regions. This mouse lacks KMO activity but also has the potential for conditionalz(tissue-specific) knockout capability. Next, a wild-type mouse line was created by crossing (and backcrossing) Kmo^{null} mice with an FLP-deleter line to excise the FRT-flanked stop signal and restore *Kmo* transcription ($Kmo^{FRT\text{-}deleted}$, hereafter referred to as Kmo^{wt}). Kmo^{null} and Kmo^{wt} mice have been described in detail previously.[10] To create hepatocyte-restricted *Kmo* knock-out mice, $Kmo^{FRT\text{-}deleted}$ mice were crossed with the *Albumin-Cre* B6.Cg-Tg (*Alb*-Cre) 21Mgn/J mice. These mice were backcrossed for at least 6 generations to generate homozygous $Kmo^{FRT\text{-}deleted}$ and *Alb*-Cre positive mice. In this line *Kmo* deletion occurs only in hepatocytes (hereafter referred to as $Kmo^{alb\text{-}cre}$ mice). The genotype of each mouse was checked by standard PCR-based genotyping of genomic DNA isolated from ear clips. The following primer sequences were used for PCR genotyping: 5′-GCGGTCTGGCAGTAAAAACTATC -3′ and 5′-GTGAAACAGCATTGCTGTCACTT-3′ to yield a single PCR product of 100 base pairs representing *Alb*-Cre positive. Mice were housed in University of Edinburgh facilities with a 12:12-h light-dark cycle. Mice were individually housed at least one day prior to experimentation, to acclimatise, and throughout the experimental time course, with standardised environmental enrichment and access to RM1 diet and water *ad libitum*. Room air temperature was maintained at ~23°C (range 20–26°C). All body weight measurements were performed under general anesthesia using a single instrument, which recorded weight in grams to 2 decimal places.

Taurocholate-induced acute pancreatitis

We modified the version of a published protocol for retrograde intraductal sodium taurocholic acid (Na-TCA) solution infusion (Perides et al., 2010). Briefly, at laparotomy under general anesthesia with isofluorane gas in oxygen, and under aseptic conditions, the biliopancreatic duct was cannulated through the transduodenal route with temporary occlusion of the proximal hepatic duct with a microclamp (Fine Science Tools 18055-06). Na-TCA (Sigma-Aldrich) in Dulbecco's PBS (Gibco) was infused at a constant rate into the duct with a pump (PHD pump). The duodenal puncture wound was closed with 7-0 Prolene (Ethicon). The concentration of sodium taurocholate injected into the pancreatic duct at laparotomy was 0.02 g/mL, with an infusate volume 50 μL, and a pump flow rate at 10 μL/min. Laparotomy closure was performed as a running mass closure of the abdominal wall with 5-0 Mersilk (Ethicon), and skin closed with 2x autoclips (Harvard Apparatus).

Telemetry implantation

Continuous clinical monitoring was performed using a radiotelemetry monitoring system. Telemetry transmitters (G2 E-Mitter), energizer/receiver pads (ER-4000) and the other hardware and data acquisition software (VitalView 5.1) were purchased from Starr Life Sciences Corporation. Aseptic surgical implantation of the telemetry transmitters was performed in anesthetized animals through an upper midline abdominal incision. After surgical implantation, the animals recovered from anesthesia in heated box (30°C). Telemeters and surgical instruments were cleaned using Enzystel (Tristel) and disinfected with Medistel (Tristel), in accordance with manufactures' instructions. Pre-emptive analgesia was given immediately prior to surgery and consisted of a subcutaneous bolus of buprenorphine (0.05 mg/kg). After midline laparotomy under general anesthesia, the telemetry device is implanted inside the abdominal cavity, and secured to the anterior abdominal wall with 5-0 Mersilk. Before closure, 0.5 mL PBS solution is given as an intra-peritoneal resuscitative fluid bolus. Wounds clips were used to close skin (Harvard Apparatus). Data acquisition software was programmed to continuously record measurements at 60-s intervals.

METHOD DETAILS

Blood preparation for flow cytometry

For analysis of the circulating blood innate immune cells population, 50 μL blood was collected from cardiac puncture and mixed 1:1 with sodium citrate aqueous (prepared as 3.8% sterile filtered) 24-h after treatment with AP induction or sham. These samples were initially maintained on ice (during transfer) and allowed to warm to room temperature. 100 μL blood-citrate mix was incubated with scientifically appropriate fluorescently labeled antibodies (see cell staining below) at room temperature, protected from light, for 20 min. Next, cells were fixed, and erythrocytes lysed by adding 450 μL of 1x RBC Lysis Buffer (BioLegend) in deionised H_2O to samples which were gently mixed and protected from light for 10 min at room temperature. Samples were then analyzed by flow cytometry.

Tissue preparation for flow cytometry

For analysis of innate immune cell populations in both lung and liver were immediately perfused with cold (~4°C) Dulbecco's PBS at time of cull by 2 × 2.5 mL via cardiac puncture, and 2.5 mL for portal vein perfusion. Harvested organs were maintained in cold (~4°C) DMEM medium during transfer to lab for immediate processing. Weights of tissue for dissociation were measured. Mouse

lung (#130-095-927) and liver (#130-105-807) dissociation kits and a GentleMACS dissociator were used to generate cell suspensions using organ-specific programs, in accordance with the manufacturer's instructions (Miltenyi Biotec). Cell concentrations were determined using an automated Nucleocounter NC-100 and NucleoCassettes, in accordance with manufacturer's instructions (ChemoMetec). Cells for staining were incubated for 30 min with a live-dead marker, Fixable Viability Dye eFluro 455 UV (eBioscience), at 2 to 8°C, protected from light, at final concentration of ~1:1000 to allow exclusion of dead cells. Cells suspensions were plated at 1 × 10^6 cells per well in a volume of 30 μL, before the addition of 50 μL (1:500 concentration) CD16/CD32 mouse BD Fc Block (BD Biosciences, #553142), to reduce non-specific binding, with an incubation for 15 min at 2 to 8°C, protected from light. Then 20 μL of multiple stains were added, making a volume of 100 μL, and incubated for 25 min at 2 to 8°C, protected from light. After multiple centrifuge spins, washings, and resuspensions in FACS buffer, formaldehyde fixation was added to give a final concentration of 2% formaldehyde.

Cell staining and flow cytometry

Cells were surface stained with fluorescently labeled antibodies to: CD3-PE (clone 17A2, BioLegend #100205), CD11B-BV421 (clone M1/70, BioLegend #101236), CD11C-PE-Cy7 (clone: N418; BioLegend #117318), CD19-PE (clone 6D5, BioLegend 115508), CD45-AF700 (clone 30-F11, BioLegend #103128), CD64-APC (clone FcγRI, BioLegend #139306), CD115-APC (clone: CSF-1R; BioLegend #135510), F4/80-APC (clone CI:A3-1, AbD Serotec #MCA497APCT), Ly6C-FITC (clone HK1.4, BioLegend #128006), Ly6G-PerCP/Cy5.5 (clone 1A8; BioLegend #127616), MHCII-APC/Fire 750 (clone I-A/I-E, BioLegend, #107652), NK1.1-PE (clone PK136, BioLegend #108708), Siglec-F-PE-CF594 (clone E50-2440; BD Bioscience, #562757). Blood leukocytes were characterised as: $CD45^+$, $lineage^-$ ($CD3^/CD19/NK1.1$), Siglec F^-, $CD11b^{hi}$, $Ly6G^{hi}$ (neutrophils); $CD45^+$, $lineage^-$ ($CD3^/CD19/NK1.1$), $CD11b^+$, Siglec F^+ (eosinophils); $CD45^+$, $lineage^-$ ($CD3^/CD19/NK1.1$), $CD11b^+$, Siglec F^-, $Ly6G^-$, $CD115^+$ (monocytes). Monocytes were further characterised as a pro-inflammatory subgroup by $Ly6C^{hi}$. Liver leukocytes were characterised as: $CD45^+$, live, $lineage^-$ ($CD3^/CD19/NK1.1$), $CD11b^{hi}$, $Ly6G^{hi}$ (neutrophils); $CD45^+$, live, $lineage^-$ ($CD3^/CD19/NK1.1$), $Ly6G^-$, Siglec F^-, $CD11b^{lo}$, $F4/80^{hi}$ (Kupffer cell monocytes); $CD45^+$, live, $lineage^-$ ($CD3^/CD19/NK1.1$), $CD11b^+$, non-neutrophils (not $CD11b^{hi}/Ly6G^{hi}$), $F4/80^{lo}$, non-DCs (not CD11c+/MHC II+) (infiltrative monocytes). Infiltrative monocytes were further characterised as a pro-inflammatory subgroup by $Ly6C^{hi}$. Lung leukocytes were characterised as: $CD45^+$, $lineage^-$ ($CD3^/CD19/NK1.1$), Siglec F^-, $CD11b^{hi}$, $Ly6G^{hi}$ (neutrophils); $CD45^+$, $lineage^-$ ($CD3^/CD19/NK1.1$), $CD11b^+$, Siglec F^+ (eosinophils); $CD45^+$, $lineage^-$ ($CD3^/CD19/NK1.1$), $CD11b^+$, Siglec F^-, $Ly6G^-$, $CD64^+$ (monocytes). Monocytes were further characterised as a $Ly6C^{hi}$ subgroup. Samples were analyzed using Fortessa LSRII flow cytometer (BD Biosciences), using stained and unstained cells, along with beads (UltraComp eBeads, eBioscience) to perform necessary prior compensations. FMO (fluorescence minus one) controls, unstained cells and heated dead cells samples were used to assist in thresholding gated populations. At the laboratory bench, the analyst was blinded to the treatments using anonymising sample codes, and data was analyzed using FlowJo software V10.1r5 (Tree Star).

Plasma cytokine assay

Blood samples were taken by cardiac blood sampling under terminal anesthesia, transferred to EDTA tubes (Microvette,CB 300 K2E, Sarstedt) and centrifuged at 5,000 rpm (2380 RCF) for 3-min (Biofuge Pico, Heraeus), and plasma frozen on dry ice and transferred to storage at −80°C. Evaluation for cytokine levels was performed with Meso Scale Discovery (Rockville) technology using V-PLEX Proinflammatory Panel1 mouse kits, run in accordance with the manufacturer's instructions. At the laboratory bench, the analyst was blinded to the treatments using anonymising sample codes and samples were run in duplicate.

Clinical biochemical assays

Plasma amylase, albumin, ALT, glucose, LDH, and urea were analyzed using commercial kits (Alpha Laboratories Ltd) adapted for use on a Cobas Fara centrifugal analyser (Roche diagnostics Ltd). At the laboratory bench, the analyst was blinded to the treatments using anonymising sample codes.

Liquid chromatography-tandem mass spectrometry (LC-MS/MS) analysis of tryptophan metabolites

Plasma samples were diluted at a 1:1 ratio with 4% phosphoric acid and internal standard(s) added as appropriate (e.g., 50 ng deuterated tryptophan; d5-tryptophan). To allow quantification, a calibration curve was made using an array of aqueous standards prepared by serial dilution (100, 50, 20, 10, 5, 2, 1, 0.5, 0.2, 0.1 ng) with the following compounds: tryptophan, kynurenine, kynurenic acid, 3-hydroxykynurenine, anthranilic acid, 3-hydroxyanthranilic acid, quinolinic acid and xanthurenic acid (Sigma-Aldrich). For both plasma and urine, the internal standard (e.g., 50 ng d5-tryptophan or d5-kynurenic acid) was added before a 1:1 dilution in 4% phosphoric acid (AnalaR, VWR) in HPLC grade H_2O (Fisher Scientific). For analysis of plasma alone, standards were first suspended in 1% bovine serum albumin (Sigma- Aldrich) as a surrogate plasma matrix. At the laboratory bench, the analyst was blinded to the treatments with the use of anonymising sample codes. Each sample and aqueous standard was transferred to a well in a 96-well plate (Waters Oasis HLB, 10 mg sorbent, 30 μm particle size) and vacuumed to dryness, washed, and dried. Extracts were washed with water and eluted with 80% methanol (HPLC grade from Fisher Scientific). The elute was dried by nitrogen gas flow at 60°C and 30 L/min. Dried extracts were re-suspended in 100 μL 30% methanol in HPLC grade water. Ten-μl volumes of each suspended extract were injected onto a column (Ace C18-PFP column; 100 × 2.1 mm internal diameter, 1.7 μm) using a Shimadzu Nexera MP UHPLC liquid chromatography system linked to a QTRAP 6500 mass spectrometer (Sciex). The flow rate was set at 0.4 mL/min at

40°C. Separation was carried out using mobile phase A – 0.1% formic acid (in HPLC grade H_2O) and mobile phase B – 0.1% formic acid (in HPLC grade methanol). Data was acquired and processed using Analyst 3.0 software ABI (Sciex). All peaks were individually checked before analysis.

Isotope tracer studies

A mixture containing 50 μg/mL tryptophan-indole-d_5 (Sigma-Aldrich) and 50 μg/mL $^{13}C_6$-3-hydroxykynurenine (Sigma-Aldrich) was made in Dulbecco's PBS (Gibco). Age-matched adult male mice from each line (*Kmo*^{null}, *Kmo*^{wt}, *Kmo*$^{alb\text{-}cre}$) were anesthetized, weighed, and a weight-adjusted dose injected intravenously by the tail vein (or penile vein as second line). After 20-min post-injection, still under anesthesia, blood was sampled by cardiac puncture and available urine sampled by urinary bladder puncture. Plasma was stored after collection in EDTA tubes (Microvette,CB 300 K2E, Sarstedt) and centrifuged at 5,000 rpm (2380 RCF) for 3-min (Biofuge Pico, Heraeus). Plasma and urine were frozen on dry ice and transferred to storage at −80°C until measured by LC-MS/MS.

Micro-osmotic pump KMOi drug study

A 50:50 mixture of DMSO:Polyethylene glycol 400 was used to dissolve a KMO inhibitor small molecule GSK898 (supplied by GlaxoSmithKline), or else DMSO:PEG-400 alone for vehicle treatment. Under sterile conditions, the reservoir (100 μL) of osmotic pumps (1002, ALZET) which were designed to administer 0.25 μL per hour for 14 days, were filled with drug or vehicle and the flow moderator fully inserted. Each pump, including moderator, was weighed before and after injection to evidence filling, and primed overnight by incubation in sterile PBS at 37°C. Mice were randomised to KMOi treatment or vehicle, and pumps implanted into the scruff of mice under short inhalational anesthesia, and under aseptic conditions, 3-days prior to induction of AP. Skin closure was performed with an autoclip (Harvard Apparatus).

Pancreas injury histology scoring

Pancreas scoring was conducted by an experience mouse histopathologist (JB) who was blinded to the mouse line and treatment allocation. The histological scoring for acute pancreatitis has been described by others and gives a total score of 0–9, with equal weighting to oedema (0–3), inflammatory cell infiltrate (0–3) and acinar necrosis (0–3).[26]

Gene expression profiling

The expression of liver, lung and spleen genes were measured by TaqMan real-time PCR using Applied Biosystems 7900HT Fast Real-Time PCR System. mRNA for Kmo (Mm01321344_m1) was monitored using commercial primer and probe sets (from ThermoFisher Scientific).

Caspase 3 and 7 activity assays

Human Lung Microvascular Endothelial Cells (HMVEC-L; #CC-2527) and Human Small Airway Epithelial Cells (SAEC; #CC-2547) were supplied by Lonza and cultured in Endothelial Cell Growth Basal Medium-2 (EBM-2) and Small Airway Epithelial Growth Medium (SAGM), respectively. Human renal proximal tubule epithelial cells (HRPTEpC; #930-05A) were supplied by Sigma-Aldrich and cultured in RenaEpi Growth Medium. 5 × 10^4 cells per well of HMVEC-L or SAEC cells, and 2.5 × 10^4 HRPTEpC cells per well were seeded on a white flat-bottomed plate with volume made up to 200 μL and incubated at 24-h at 37°C, 5% CO_2. 20 μL medium was discarded from each well and 20 μL of treatment medium was then added to each designated well. Treatments comprised individual metabolites: tryptophan, kynurenine, kynurenic acid, 3-hydroxykynurenine, 3-hydroxy-anthranilic acid and xanthurenic acid or quinolinic acid (Sigma-Aldrich) with or without cytokines. Cytokine treatments comprised human interleukins-1β, −6 or −10 (Miltenyi Biotec). All metabolites were dissolved in sterile filtered dimethyl sulphoxide (DMSO from Sigma-Aldrich). For HMVEC-L studies, a final concentration of 0.5% DMSO (vol/vol) to cells was used, including caspase-activator control Staurosporin (Sigma-Aldrich #S5921). Because pilot data showed DMSO-induced toxicity at 0.5% in SAEC cells, the concentration was reduced to 0.2% DMSO (vol/vol) for SAEC and HRPTEpC cells. Plates were gently agitated to mix, and cells incubated with treatments for 4-h at 37°C, 5% CO_2. 100 μL supernatant was discarded and 100 μL of Caspase-Glo reagent (Promega #G8091) was added to each well. Plates were gently mixed and incubated at 37°C, 5% CO_2 for 90-min for HMVEC-L or SAEC, and 105 min for HRPTEpC cells. For HMVEC-L studies, luminescence was read on an automated Tecan Infinite M1000 plate reader with OD1 attenuation and a 1000 ms integration time, and for SAEC and HRPTEpC cells a Promega Glomax Multi+ Detection system was used to quantify luminescence, with a 500 ms integration time.

Cell viability assay

SAECs were cultured in SAGM and seeded at 5 × 10^4 cells per well in a transparent flat-bottomed plate and made up to 200 μL. HRPTEpCs were seeded at 2.5 × 10^4 cells per well in a transparent flat-bottomed plate using RenaEpi Growth Medium and made up to 200 μL. Seeded plates were incubated for 24-h at 37°C, 5% CO_2. 20 μL medium was discarded from each well and 20 μL of treatment medium was then added to each designated well. Treatments comprised individual metabolites: tryptophan, kynurenine, kynurenic acid, 3-hydroxykynurenine, 3-hydroxy-anthranilic acid and quinolinic acid (Sigma-Aldrich) with or without human interleukins-1β (Miltenyi Biotec). All metabolites were dissolved in sterile filtered in 0.2% DMSO (vol/vol) to cells. Wells were gently mixed before re-incubation at 37°C, 5% CO_2 for 24-h. Thereafter, for each well, 100 μL supernatant was removed before the addition

of 10 μL Alamar Blue cell viability assay reagent (ThermoFisher). Plates were gently agitated to mix, and a 2-h incubation at 37°C, 5% CO_2 completed. Fluorescence was read on a Promega Glomax Multi+ Detection system, using green fluorescence filter (Ex 525, Em 580–640).

QUANTIFICATION AND STATISTICAL ANALYSIS

Telemetry data processing for visualization

Telemetry data was stored as comma-separated value (CSV) files using VitalView (version 5.1). Data recording began from the midpoint of the light-phase (see Figure 3D) which was denoted as zeitgeber time 0-h (ZT0) to align recorded behaviors of interest (activity and temperature) as these are under circadian regulation. Data files were processed using open-source scientific tools for Python using the Anaconda Software Distribution (version 2–2.4.0.) The Python program code, which specifies the Python libraries utilised, and the primary telemetry CSV files, are available on a Github repository at the following URL: https://github.com/HayesAJ83/HayesMole_CellRep.git. The program code was used to produce data visualisations in Figures 3E, 3F and 4P.

Telemetry data statistical data analysis

Rolling average hourly mean core body temperature measurements $Y_{m\,j}$ were calculated for each mouse m at hour j. The first 11 h of telemetry data (from ZT0 to ZT11, i.e., 13:00-h to 24:00-h) were removed from calculations as this early post-operative period had marked altered variability that would impair analyses. To estimate variability for each mouse, the following equation was used:

$$W_{m\,j} = \left[Y_{m\,j} - \frac{Y_{m\,j+1} + Y_{m\,j-1}}{2} \right] \sqrt{2/3}$$

and the standard deviation was estimated robustly as the median absolute deviation of $W_{m\,j}$ for every third j, to avoid dependence. The first and the last observations were excluded. These standard deviations are plotted in Figure 3K.

A collective physiological recovery profile, using the Kmo^{wt} sham control group mice, was calculated to define prediction band within which recovery data from this group are expected to lie (with 0.05 α level) which are defined as:

$$\left\{ Y_j^{new}, j \in 1:J : \left| \overline{Y}_{Group\,j} - Y_j^{new} \right| \leq \sqrt{\left(1 + \frac{1}{|Group|}\right)} * \widehat{\sigma}_{Group} * t_s \left((1-\alpha)^{1/J} \right) \text{ for all } j \in 1:J \right\}$$

where $\overline{Y}_{Group\,j}$ is the mean at hour j among the mice in the considered group (e.g. Kmo^{wt} sham), $|Group|$ is the number of mice in the considered group, J is the number of hourly observations per mouse, $t_s(\alpha)$ is (1-α)100% quantile of Student's t distribution with s degrees of freedom, $s = (|Group|-1) * J$, and

$$\widehat{\sigma}^2_{Group} = \frac{1}{J\,(|Group| - 1)} \sum_{j \in 1:J} \left[\sum_{m \in Group} (Y_{mj} - \overline{Y}_j)^2 \right]$$

This formula works under the assumption that the variance is the same for each time point and for each mouse within the group, and that the observations have normal distribution. Control prediction bands are shown in Figures 3I and 3J as dotted red error bars.

RNA-seq data analysis

RNA sequencing (RNAseq) data analysis was performed as follows: Firstly, data quality checks were completed with FastQC (version 0.11.7). Read trimming was performed with Trimmomatic (version 0.36) with java/jdk (version 1.8.0). RNA-seq read alignment was performed with STAR (version 2.5.3a). Read counting was performed with featureCounts (Subread version 1.5.2). Differential gene expression analysis between conditions and likelihood ratio tests (to select top genes) were performed with DESeq2 (version 1.20) with R (version 3.5.0). For visualisation purposes, data was transformed using rlog in DESeq2 (log2 transformation and library size-normalisation) and row scaling was applied ((value - mean)/sd). Reactome pathway analysis and visualisation were performed using ReactomePA.[25] Metabolomics data were analyzed using MetaboAnalyst (v3.0).[69] Pre-processing consisted of quantile normalisation, log transformation and mean-scaling. The tests chosen for the pathway analysis were 'global test' and 'relative-betweenness centrality test' and KEGG data was used.

Statistics and power analyses

Conformity of data to the normal distribution was assessed by one-sample Kolmogorov-Smirnov with Lilliefors Significance Correction and Shapiro-Wilk tests. The Levene statistic was used to test homogeneity of variance between groups. Two group data that were normally distributed were compared by unpaired *t* test, and non-parametric two-group data were compared by the Mann-Whitney U test. Multiple groups of normally distributed data were compared by ordinary one-way analysis of variance (ANOVA). Where significant, pairwise *post hoc* comparisons were performed by Tukey's multiple comparison test if the data met the homogeneity of variance assumption, or by Games-Howell test where the data had unequal variances. Multiple groups including non-parametric data were tested by Kruskal-Wallis H test and *post hoc* pairwise comparisons made using the Dunn-Bonferroni approach.

two-way ANOVA was used to compare two categorical variables on a continuous variable. All statistical tests were based on a two-sided α-value of 0.05. Comparison of survival curves was conducted with Log rank (Mantel-Cox) test.

Power calculations were performed using G*Power (v3.1.9.4) software. A priori analysis was performed where suitable data were available, otherwise post hoc power calculations were performed. The following input parameters were routinely used: 2-tailed, α error probability of 0.05, and power (1-β error probability) $\geq$ 0.9. Cohen's measures for the effect size *d* were determined with group means and standard deviations. Specifically, qRT-PCR (Figure 1B) sample size and power calculations were assessed *post-hoc* from mean values and standard deviations using liver *Kmo* gene expression values [Log10(2^-ddCT)] between *Kmo* deleted mice, Kmo^{null} (mean = 2e-10, SD = 0.7757) and liver-restricted knockout mice, $Kmo^{alb\text{-}cre}$ (mean = 1.332; SD = 0.157), giving an effect size *d* = 2.38 and power 0.96. Regarding metabolite concentrations, effect and sample size were used to calculate power *post-hoc* from mean values and standard deviations using concentrations of kynurenine, the substrate of KMO enzyme, between *Kmo* deleted mice, Kmo^{null} (mean = 61.4 μM, SD = 20.3 μM) and liver-restricted knockout mice, $Kmo^{alb\text{-}cre}$ (mean = 24.8 μM; SD = 6.6 μM), giving an effect size *d* = 2.42 and the power 0.96. The effect and sample size were used to calculate power mouse weights (Figure S2E) initially from n = 10 per group (three groups): *d* = 0.75, with a power 0.95, gave a sample size n = 33. For 24-h analysis, post-hoc analysis on available data from blinded histological scoring (Kmo^{wt} n = 16, and $Kmo^{alb\text{-}cre}$ n = 14), revealed an adequately powered experiment, with *d* = 0.815, giving a power 0.93. Blood samples from these same subjects were used for amylase testing, which on *post-hoc* analysis were sufficiently sized cohorts to power the experiment sufficiently, with a power 0.95. For consistency, these same subjects were used for testing albumin, glucose, ALT, LDH and urea (supplementary 4E-4I). In line with 3Rs, all efforts to maximise yield of samples was made from the outset, and as there were separate groups of mice used for multi-organ histological storage and other groups used for multi-organ flow cytometry, there were greater numbers of subject with stored plasma available for measurement of circulating cytokine concentrations than for histology alone. Specifically, there was up to n = 11 for all groups. *Post-hoc* power analysis using Kmo^{wt} sham and AP data, calculated *d* = 1.672 and gave a power 0.96 with n = 11. Data were analyzed using IBM SPSS Statistics version 23.0 (IBM Corp., Armonk, NY, USA) and GraphPad Prism v7.0. *p* values $\leq$0.05 were considered statistically significant.